Image Cover Sheet

CLASSIFICATION	SYSTEM NUMBER
UNCLASSIFIED	148750

TITLE

EXPERIMENTAL MEASUREMENTS OF CONCENTRATION FLUCTUATIONS AND SCALES IN A DISPERSING PLUME IN THE ATMOSPHERIC SURFACE LAYER OBTAINED USING A VERY FAST RES

System Number:

Patron Number:

Requester:

Notes:

DSIS Use only:

Deliver to: FF

Reprinted from JOURNAL OF APPLIED METEOROLOGY, Vol. 33, No. 8, August 1994
American Meteorological Society

Experimental Measurements of Concentration Fluctuations and Scales in a Dispersing Plume in the Atmospheric Surface Layer Obtained Using a Very Fast Response Concentration Detector

EUGENE YEE

R. CHAN AND P. R. KOSTENIUK

G. M. CHANDLER

C. A. BILTOFT AND J. F. BOWERS

Experimental Measurements of Concentration Fluctuations and Scales in a Dispersing Plume in the Atmospheric Surface Layer Obtained Using a Very Fast Response Concentration Detector

EUGENE YEE

Defence Research Establishment Suffield, Medicine Hat, Alberta, Canada

R. CHAN AND P. R. KOSTENIUK

Kosteniuk Consulting Ltd., Saskatoon, Saskatchewan, Canada

G. M. CHANDLER

S & J Engineering, Inc., Scarborough, Ontario, Canada

C. A. BILTOFT AND J. F. BOWERS

Meteorology Division, Materiel Test Directorate, U.S. Army Dugway Proving Ground, Dugway, Utah

(Manuscript received 3 May 1993, in final form 22 December 1993)

ABSTRACT

High-frequency fluctuations of concentration in a plume dispersing in the atmospheric surface layer have been measured with high-resolution concentration detectors (approximately 270 Hz at the −6-dB point) to extract various concentration statistics of the fluctuating concentration field. Crosswind and alongwind variations of amplitude statistics (e.g., the total and conditional fluctuation intensity, skewness, and kurtosis), the intermittency factor, and the shapes of the concentration probability density function (PDF) are presented. The behavior of temporal concentration statistics such as the autocorrelation function; power spectrum; PDF of upcrossing intervals; PDF of excursion durations; various concentration timescales, length scales, and microscales (e.g., Taylor microscale, correlation scale, length scale based on the spectral peak, etc.); as well as the velocity-to-concentration timescale ratio are studied. It is shown that all the concentration length scales and microscales (with the exception of the correlation scale) grow with downwind distance in proportion to the mean plume width.

1. Introduction

The nature of fluctuations in concentration of a passive scalar (e.g., pollutant contaminant) released into the turbulent flow field of the atmospheric surface layer is of critical importance in many industrial and environmental fluid mechanics problems, ranging from air quality control and regulation of hazards posed by the release of highly toxic or flammable gases to an understanding of fast nonlinear physicochemical processes required for the design of efficient mixing and combustion devices. Recently, interest in the prediction of expected concentration fluctuation levels in plumes dispersing in the atmosphere has experienced a renaissance. While the need to develop statistical models for the description of potential hazards resulting from the accidental release of toxic or flammable gases into the atmosphere has been recognized for quite some time (e.g., Gifford 1959; Csanady 1967; Chatwin 1982), fast-response concentration sensors required for the measurement and characterization of the fluctuating concentration field have not been available until recently. This development of fast-response detectors has generated renewed interest in the detailed structure of dispersing plumes.

Laboratory measurements of concentration fluctuations in a wind tunnel or water channel have been made by Fackrell and Robins (1982a), Stapountzis et al. (1986), Deardorff and Willis (1988), and Bara et al. (1992). Although laboratory experiments have provided the most extensive measurements of statistics in a dispersing plume to date, they are limited in the sense that the full range of large-scale eddy motions in the atmosphere and atmospheric conditions (e.g., diabatic conditions such as extreme stable stratification) cannot be properly modeled. Consequently, a number of full-

Corresponding author address: Eugene Yee, Defence Research Establishment Suffield, Box 4000, Medicine Hat, Alberta, T1A 8K6, Canada.

scale atmospheric field experiments have been undertaken in recent years to study the turbulent fluctuations in concentration in a dispersing plume (e.g., Hanna 1984; Sawford et al. 1985; Sawford 1987; Dinar et al. 1988; Peterson et al. 1990; Mylne and Mason 1991; Mylne 1992; Yee et al. 1993a,b). In spite of these efforts, comprehensive and reliable data on the fluctuating concentration field obtained from atmospheric experiments are still comparatively rare and certainly have not provided information as complete as laboratory experiments on the statistical characteristics of concentration fluctuations.

This paper reports on an experimental investigation of the statistical characteristics of dispersing plumes in the atmosphere measured with very fast response concentration detectors. Among quantities studied are the concentration power spectra; correlations; length scales, timescales, and microscales; intermittency factor; higher-order moments of concentration; probability density functions of concentration; upcrossing intervals; and excursion durations. We have used the data to try to better understand the physical mechanisms responsible for turbulent diffusion, but we envisage that the data will eventually be useful in the development of statistical models for calculating atmospheric dispersion required for practical hazard assessments and operational or regulatory applications.

2. Experimental procedures

All measurements used in the present study were carried out in September 1991 and November 1992 as part of a cooperative Concentration Fluctuation Experiments (CONFLUX) project involving three defense research establishments in the United States, United Kingdom, and Canada. The field experiments were conducted near Tower Grid on U.S. Army Dugway Proving Ground, Utah (40°06′N, 112°59′W), about 2 km west of Camel Back Ridge on the edge of the Great Salt Lake Desert. The terrain was uniform and homogeneous, covered with short grass interspersed with a few low shrubs that are less than 0.5 m in height, providing an upwind fetch that is absolutely uniform and unobstructed for 5 km or more. We used wind speed and momentum flux measurements from three-axis sonic anemometers in conjunction with Monin–Obukhov similarity relations to determine a site roughness length z_0 of about 0.015 m.

The meteorological instrumentation deployed during the field experiments conducted in September 1991 (Phase I) has been described in some detail by Biltoft (1991). The siting of the instrumentation masts to form the measurement array and the prevailing atmospheric conditions for each of the field trials conducted during Phase I of the CONFLUX project are also described in the same reference. The experimental system used to measure concentration fluctuations in a dispersing plume as well as a preliminary analysis of the concentration fluctuation datasets obtained from Phase I using this system have been described in detail by Yee et al. (1993a). The field experiments carried out in November 1992 (Phase II) used the same grid design, but the sampling line of instrumentation masts was much longer than that used during Phase I. Briefly, the sampling line used during Phase II consisted of 18 3-m masts and 2 9-m meteorological masts oriented at 45° from true north to take advantage of prevailing nighttime and daytime winds from 135° and 315°, respectively. Sonic anemometer/thermometers (Applied Technologies, Inc.) were mounted at heights of 4 and 8 m above the ground on each of the two meteorological masts. Fiber-optic quartz thermometers (TACAN/IPITEK Corp.) were installed at 2, 4, 6, and 8 m on each of the meteorological masts to provide temperature profile measurements. The data from the sonic anemometers and fiber-optic quartz thermometers were sampled at 10 and 1 Hz, respectively, with a computer-controlled digital data acquisition system. Data were stored on flexible removable hard drives (Iomega Corp.). In addition, horizontal wind component data across the field site were collected over two perpendicular 300-m optical paths formed between transmitter and receiver pairs of two spatially averaged filter scintillometers developed by the National Oceanic and Atmospheric Administration Wave Propagation Laboratory.

Propylene (C_3H_6) tracer gas was released at a constant rate as a point source at a height h of 2.5 m. The gas dissemination system consisted of two propylene cylinders connected in parallel and immersed in a hot-water bath. A Matheson 1L-510 regulator was connected to the outlet of the cylinders to ensure a constant downstream pressure, and a flexible hose was used to connect the regulator to the inlet fitting of the mass flow controller (Teledyne Hastings-Raydist). This controller, which consisted of a sensor, electronic circuitry, a shunt, and a valve, was used to set, control, and measure the flow rate of gas through the dissemination system. The controller allowed a constant gas flow rate to be maintained at a user-selected reference level (between 1.67×10^{-4} and 3.76×10^{-3} m^3 s^{-1}) to within about 2%. A quick-release connector mated the outlet fitting of the mass flow controller to the dissemination hose, which was connected to the base of the disseminator, a section of schedule 40 PVC (polyvinyl chloride) pipe 1 m in length and 0.05 m in diameter.

The concentration analyzers were modified versions of a photoionization detector (TIP) manufactured commercially by Photovac, Inc. (Thornhill, Ontario, Canada) as a handheld detector for air quality monitoring. Our modifications to the standard TIP detector have improved its reliability and robustness for full-scale atmospheric field experiments as well as its overall response characteristics and sensitivity for measure-

ments of the fluctuating concentration field. Up to 10 fast-response concentration sensors, which we call TIP-SJs, were used during Phase I, and 22 improved fast-response concentration detectors, which we call TIP-SJ2s, were used during Phase II of the CONFLUX project. Because there is currently no concentration detector that is capable of resolving the finest scales existing in concentration fluctuations in a dispersing plume in the atmosphere, it is important to specify the response characteristics of the detector to meaningfully compare measurements of fluctuation statistics made by various researchers using instruments at different resolutions and to assess the effect of instrument smoothing on the perceived concentration fluctuations. Indeed, Mole (1990) and Chatwin and Sullivan (1993) have emphasized the importance of accounting for the effects of instrument smoothing on the analysis and interpretation of concentration fluctuation data. In view of this, we have characterized the response time of our detectors by delivering a narrow pulse of gas to the sampling inlet of the detector with a swinging pendulum apparatus that allowed a controlled propylene air jet to exit from its end. The TIP-SJ detector has a response time of about 0.01 s, implying that its frequency response falls 6 dB at about 100 Hz from its dc level; the TIP-SJ2 detector has a response time of about 0.0037 s (viz., the −6-dB point of the frequency response was about 270 Hz). The detection limits of the TIP-SJ and TIP-SJ2 analyzers were 0.1 parts per million (ppm) and 10 parts per billion (ppb), respectively. The concentration detectors were placed along the sampling line of fixed masts at a sampling height z of 3 m above ground to provide a straight line in the crosswind direction through the plume. A complete description of the TIP-SJ and TIP-SJ2 detectors can be found in Chandler (1991) and Chandler (1993), respectively.

The data acquisition system for the concentration data was preceded by antialiasing eight-pole Butterworth filters and amplifiers. Data were sampled with an i486 PC-controlled, high-speed, high-resolution 16-bit analog-to-digital (A/D) input–output board and multiplexer (HSDAS 16 and SMUX 64, Analogic Inc.) and stored on a high-capacity external disk drive (1.75 GB) as 16-bit unsigned integers in multiplexed form. The dynamic range of the converter is 96 dB (=65 536), allowing the accurate representation of the instantaneous concentration, which was found to span about four decades in amplitude. The raw data from the A/D converter were then demultiplexed, compressed, and archived onto 525-MB QIC (quarter-inch cartridge) data cartridge tapes. These data were later uploaded from the QIC tapes to a Hewlett-Packard 9000 Series 700 computer, where all data reduction was done. The sampling period for the concentration data ranged from 16 to 64 min for experiments conducted during Phase I and 30 min for experiments conducted during Phase II.

3. Initial data processing of concentration time series

Preprocessing of the concentration data began with the drift correction to the baseline level of each concentration time series to remove any slow variations in this level over the sampling period. Each time series was divided into M segments of length L (i.e., $M = N/L$, where N is the number of data points in the time series), with L chosen to ensure that the baseline level changed by less than one A/D unit over each segment. The concentration mean and standard deviation were then determined for each segment. Assuming that data segments with no signal present have the smallest standard deviations, a baseline threshold was chosen at about four times the minimum of the segment standard deviations. This threshold was used to identify the data segments of the concentration time series that contained noise only (viz., these segments contained no rapid fluctuations of significantly nonzero concentrations). Once the noise baseline segments were identified, the drift represented by these segments was approximated by least-squares fitting cubic splines to their mean levels and then subtracting the resulting curve from the recorded time series. Next, the resulting concentration time series (in A/D units) was converted to absolute concentration (ppm) by least-squares fitting a second-degree polynomial to the corresponding calibration curve and applying this polynomial to the data. Finally, the calibrated concentration time series was low-pass filtered on the computer with a zero-phase Butterworth filter of order 8 with the −3-dB cutoff frequency set at 250 Hz (viz., the amplitude response of the filter has a roll-off of 160 dB per decade above 250 Hz) to reduce the effects of high-frequency noise.

Following baseline and calibration correction and high-frequency noise removal, a concentration threshold χ_T required to distinguish real concentration signals from instrumental noise in the (level) baseline was determined by constructing a curve of intermittency factor γ versus concentration threshold χ_T. Here, γ is defined as the fraction of the total time in which significantly nonzero concentrations are observed (i.e., concentrations that exceed a selected concentration threshold). The selection of a concentration threshold for the determination of γ is used here in conformity with most other fluctuation studies (e.g., Mylne and Mason 1991; Bara et al. 1992), but it should be emphasized that the shortcomings of this standard definition of the intermittency have been discussed by Chatwin and Sullivan (1989). Figure 1 shows typical experimental data illustrating the variation of γ with χ_T. This curve provides quantitative information on the sensitivity of intermittency to the choice of a threshold. For very small concentration thresholds, the intermittency is near unity. The negative concentra-

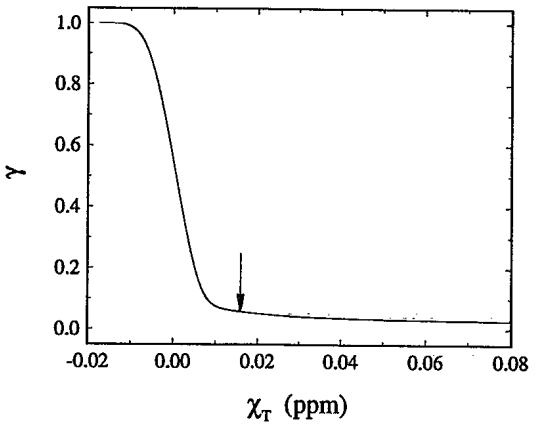

FIG. 1. Effect of the concentration threshold χ_T on the intermittency factor γ obtained from a sample concentration time series. The arrow marks the selection of the concentration threshold ($\chi_T \approx 0.016$ ppm) chosen to define the true intermittency factor for the concentration time series.

tions shown in Fig. 1 result from the baseline correction that sets the nominal zero concentration level at approximately half the amplitude range of the noise. As the threshold ranges over amplitude levels corresponding to the baseline noise, the intermittency exhibits a very sharp decrease until the threshold is increased just above the noise level, at which point the intermittency transitions to a gently sloped plateau. The concentration threshold was selected at the point at which this plateau was first attained (e.g., as indicated by the arrow in Fig. 1), and the value of γ corresponding to this threshold was taken to represent the true intermittency value. Although the intermittency shows little sensitivity to the choice of threshold in the plateau region, further increase in the value of χ_T much beyond this point would decrease the signal content of the thresholded concentration time series.

With the selection of χ_T, the final stage of the initial data processing consisted of removing the noise on the baseline. This was accomplished by applying the following nonlinear filter to each concentration data point:

$$\chi^f(t_i) = \delta_\lambda[\chi(t_i)], \quad i = 1, 2, 3, \cdots, N, \quad (1)$$

where $\chi(t_i)$ is the instantaneous concentration measured at time t_i, λ is chosen to be χ_T, and $\delta_\lambda(y) \equiv \max(0, y - \lambda)$. Henceforth, for simplicity, we use χ to denote both the random instantaneous concentration and a value assumed by this random variable. Hence, the corrected concentration data point $\chi^f(t_i)$ is obtained by pulling down every measured observation $\chi(t_i)$ by an amount λ, taking care to ensure a nonnegative result (recall that after the baseline correction, the nominal zero level of concentration corresponds approximately to a level in the midrange of the baseline noise). Computer simulations with synthetically generated data have shown that this nonlinear filter results in substantial improvements in the signal-to-noise ratio (SNR) for highly intermittent signals consisting of a few peaks (bursts) standing out from a constant noise background. It should be noted, however, that most of the time series analyzed here possessed good SNR, so application of this nonlinear filter had only a very small effect on the results. In short, this nonlinear filter affected the results significantly in only a few time series where concentrations were near zero for a large fraction of the time (e.g., time series measured at the extreme plume fringes), but this filter was applied to all the time series to ensure an overall consistency in the preprocessing of the data.

In the following sections, we focus primarily on presentation of results from the analysis of concentration data measured during Phase II of CONFLUX. The results of a preliminary analysis of concentration data obtained during Phase I have been described in detail by Yee et al. (1993a; hereafter YKCBB) and will be used as the basis for comparison with the results obtained from the more comprehensive experiments (e.g., longer crosswind sampling lines, greater downwind range) conducted during Phase II.

4. Concentration time series and amplitude concentration statistics

a. *Concentration time series*

To illustrate various features of concentration fluctuations in a dispersing plume, we have selected three 30-min field trials conducted during November 1992 under near-neutral conditions (i.e., $|z/L| \leqslant 0.02$, where L denotes the Monin–Obukhov length). Data summaries of wind velocity and turbulence statistics for these trials, obtained using a three-axis Applied

TABLE 1. Summary of wind velocity and turbulence statistics measured with three-axis sonic anemometer at the 4-m height. All turbulence statistics were averaged over 30-min sampling times. Here, x is downwind distance; h is the source height (2.5 m); U is mean wind speed; σ_u, σ_v, and σ_w are the standard deviations of wind velocity fluctuations in the alongwind (x), crosswind (y), and vertical (z) directions, respectively; $\overline{u'v'}$ and $\overline{u'w'}$ are two components of the Reynolds stress or momentum flux; and L is the Monin–Obukhov length.

Trial	Date (1992)	$\frac{x}{h}$	U (m s^{-1})	σ_u (m s^{-1})	σ_v (m s^{-1})	σ_w (m s^{-1})	$\overline{u'v'}$ (m^2 s^{-2})	$\overline{u'w'}$ (m^2 s^{-2})	L (m)
23	21 November	92	3.3	0.664	0.401	0.263	0.0046	−0.0636	139
25	23 November	74	5.3	0.826	0.577	0.340	−0.0215	−0.0783	−384
27	23 November	24	5.6	1.030	1.042	0.429	0.0798	−0.1611	−154

Technologies sonic anemometer located at the 4-m height, are presented in Table 1. Here, σ_u, σ_v, and σ_w are the standard deviations of wind velocity in the alongwind (x), crosswind (y), and vertical (z) directions, respectively; U is the mean wind speed; and $\overline{u'w'}$ and $\overline{u'v'}$ are two components of the Reynolds shear stress (momentum flux).

Figures 2 and 3 show sample concentration time series measured by detectors at two points in horizontal cross sections through a dispersing plume at nondimensional downwind fetches of $x/h = 24$ and 92, respectively. These time series are obtained from runs 27 and 23, respectively. The instantaneous concentration χ exhibited in Figs. 2 and 3 has been normalized by the source emission rate Q for the associated experiment. All the time series show both in-plume turbulent fluctuations resulting in rapidly varying concentrations and plume meandering (intermittency) resulting in periods of essentially zero concentration, but it is evident that the relative contribution of each of these components to the fluctuations depends strongly on receptor position (e.g., downwind range and crosswind location) and on atmospheric conditions (e.g., wind speed and turbulence characteristics). The concentration time series provide a strong visual indication of the wide range of timescales that are responsible for the complex concentration patterns resulting from a plume exposure at any fixed receptor.

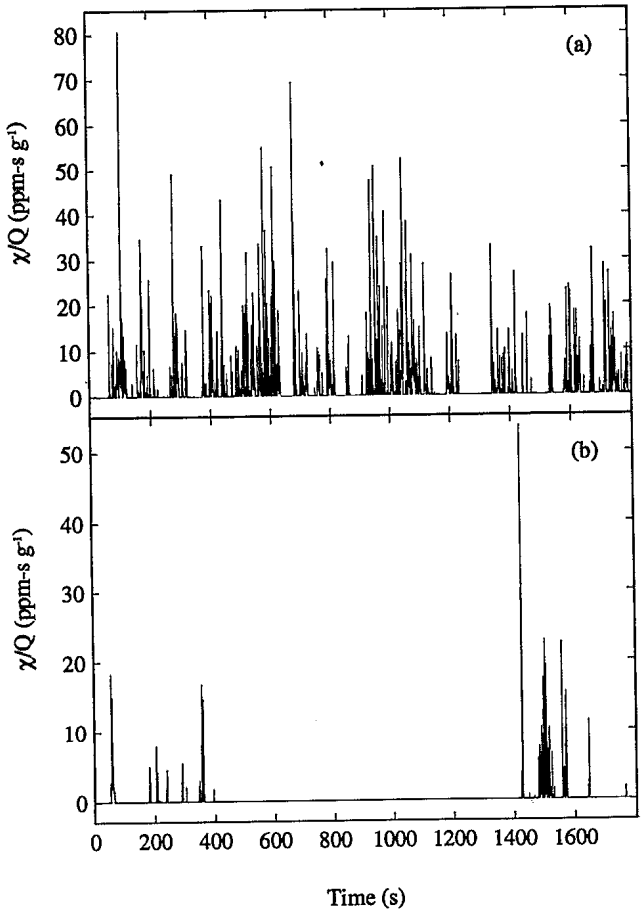

FIG. 2. Sample concentration time series for trial 27 measured at (a) $|y|/\sigma_y = 0.62$ and (b) $|y|/\sigma_y = 2.7$ at a nondimensional downwind distance $x/h = 24$. The instantaneous concentration χ has been normalized by the source emission rate Q. The time series shown here are plotted after baseline correction, calibration, and noise removal.

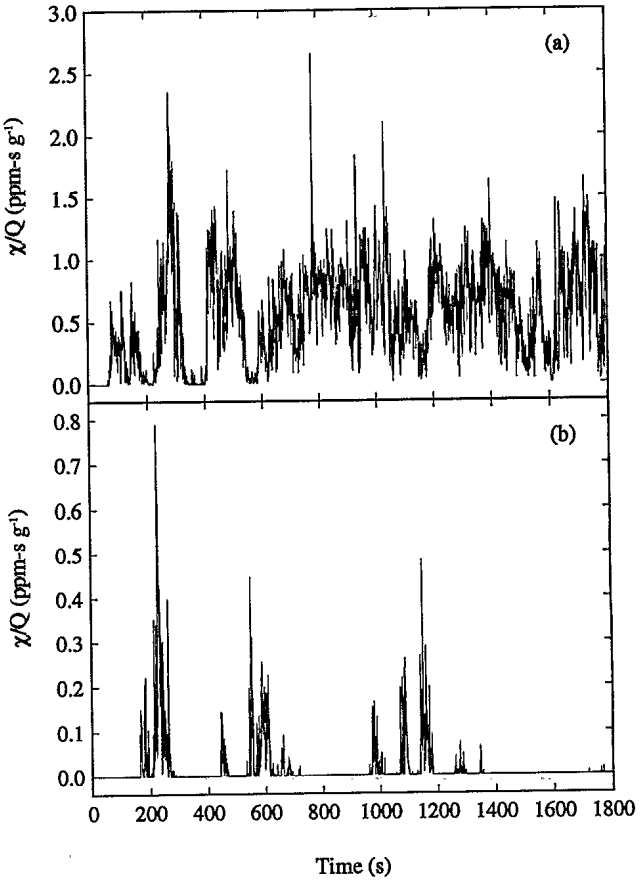

FIG. 3. Sample concentration time series for trial 23 measured at (a) $|y|/\sigma_y = 0.25$ and (b) $|y|/\sigma_y = 1.3$ at a nondimensional downwind distance $x/h = 92$. The instantaneous concentration χ has been normalized by the source emission rate Q. The time series shown here are plotted after baseline correction, calibration, and noise removal.

The time series in Fig. 2a was measured in the vicinity of the mean plume centerline (viz., at $|y|/\sigma_y = 0.62$, where y is the crosswind distance from the mean plume centerline and σ_y is the mean plume dispersion) at a downwind range of $x/h = 24$. It illustrates a concentration pattern that consists of a series of variable duration bursts of rapidly varying concentration, punctuated with randomly occurring periods of essentially zero concentration in which the plume itself most likely meandered horizontally off the receptor in response to the larger turbulent eddies. Although periods of zero concentration as long as 100 s can be observed in this time series, we note that the majority of the

zero-concentration periods are of the order of a few seconds (and consequently are not well resolved in Fig. 2a). Indeed, the clusters of bursts in the time series are sharp and short and return to zero concentration frequently. In this example, the standard deviation of wind azimuth σ_θ was only about 10°, and, in consequence, the concentration pattern that was measured simultaneously at a fixed receptor located about 30 m in the crosswind direction from that of Fig. 2a (i.e., toward the edge of the mean plume at $|y|/\sigma_y = 2.7$) exhibits relatively fewer concentration events with (on average) much longer zero concentration periods between events (e.g., Fig. 2b).

In contrast, the concentration time series shown in Fig. 3a (measured near the mean plume centerline at $|y|/\sigma_y = 0.25$ at a downwind distance of $x/h = 92$) exhibits a very high intermittency factor ($\gamma \approx 0.90$). The high-frequency structure of in-plume concentration variations, resulting from the various entraining and contorting processes that mix ambient clean air with contaminant parcels, is readily evident. In comparison to Fig. 2a, the internal fluctuations are more smoothed out with the result that the concentration bursts consist of longer periods of nonzero concentration that fall to zero less frequently. In this example, plume meandering was present, as can be seen by comparison of the time series in Fig. 3a with that in Fig. 3b, the latter of which was measured simultaneously at a receptor displaced laterally from the one in Fig. 3a by 42 m (i.e., at $|y|/\sigma_y = 1.3$). In this experiment, the wind azimuth standard deviation was about 7°, and Fig. 3b shows an example of plume exposure off the mean plume centerline where the receptor may have been impacted more frequently by the instantaneous plume edge than by its centerline (viz., the entire instantaneous plume was not swept completely over the receptor as in Figs. 2a and 2b). Based on this consideration, it was judged that the instantaneous plume width in this example was comparable to the length scale of the plume meander. In consequence, a sampling point located on the centerline of the mean plume would lie almost completely within the instantaneous plume boundary for the entire sampling period as the instantaneous plume meandered back and forth across the receptor (cf. Fig. 3a).

b. *Fluctuation intensity, higher moments, intermittency*

Crosswind profiles of the mean concentration C are given in Fig. 4a for $x/h = 24$, 74, and 92 (runs 27, 25, and 23, respectively). Each mean concentration cross-section has been normalized by its largest value, C_0. Following the usual practice, crosswind distance y from the mean plume centerline is normalized by the mean plume dispersion σ_y and centered on the mean wind direction as determined from the sonic anemometers. The mean plume dispersion was determined from the

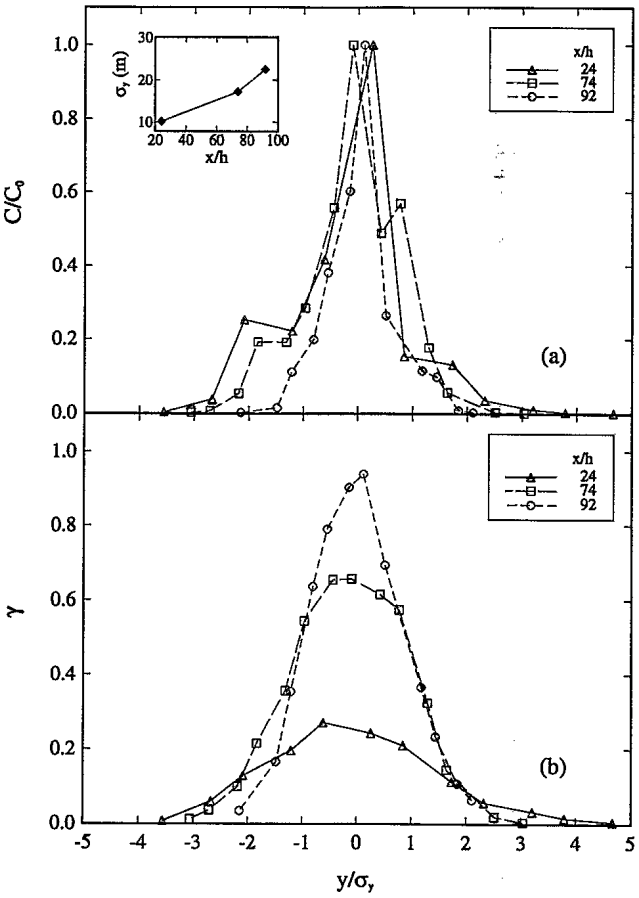

FIG. 4. Crosswind profiles of (a) mean concentration C normalized by the maximum mean concentration C_0 and (b) intermittency factor γ measured at three nondimensional downwind distances x/h. Inset in (a) shows the mean plume dispersion σ_y used to normalize the crosswind distance y plotted against the normalized downwind distance x/h.

measured turbulence statistics using the standard relationship $\sigma_y = \sigma_v x f(x)/U$, where $f(x)$ is a dimensionless function of downwind distance whose parametric form is described by Pasquill and Smith (1983). The mean plume dispersion σ_y used in the normalization of the crosswind distance y is displayed in the inset of Fig. 4a as a function of x/h.

Figure 4b shows the crosswind profiles of the intermittency factor γ at various downwind distances. The intermittency factor exhibits a considerable variation with downwind distance from the source. It attains a maximum at the mean plume centerline, where the instantaneous plume has the highest probability of being present over a receptor, and decreases to zero at the outer fringes of the plume, where the instantaneous plume is absent most of the time. Furthermore, these examples show that γ increases along the mean plume centerline with increasing fetch downwind, from approximately 0.25 at $x/h = 24$ to 0.90 at $x/h = 92$. The crosswind profiles of γ are approximately symmetric and appear to be approximately Gaussian in form,

suggesting that, at any given time, the probability of observing the meandering instantaneous plume at a distance y from the mean plume centerline can be approximated by a Gaussian distribution.

In spite of the high-frequency resolution of our sensors (e.g., approximately 270 Hz at the −6-dB point), we emphasize that the convoluted interface separating contaminant and clean-air regions in the dispersing plume contains variations at scales smaller than our resolution limit, and, in consequence, these variations will appear mixed to our detectors. Hence, our measurements of intermittency profiles should be interpreted as upper bounds on the true values obtained from an ideal detector that can resolve all scales. Keeping this in mind, our observations of the crosswind variations of γ are qualitatively similar with those observed elsewhere (e.g., Hanna 1984; Dinar et al. 1988; Mylne and Mason 1991; Bara et al. 1992). In comparing and contrasting intermittency profiles measured in various laboratory and field experiments, however, it is important to recognize the factors that could affect the absolute values of the observed intermittency, such as the ratio of the source size to the integral length scale of turbulence (Fackrell and Robins 1982b; Chatwin and Sullivan 1979), the instrument resolution and sensitivity, and the threshold used to define the intermittency. The maximum mean plume centerline value of γ measured at 60 m under near-neutral conditions is about 0.3, and this is consistent with results reported by YKCBB at similar range (50 m) and by Mylne and Mason (1991). However, our experiments at about 200 m in near-neutral conditions exhibit mean plume centerline γ values of about 0.9, whereas Mylne and Mason (1991) observe values between about 0.4 and 0.5 at similar ranges. The differences are most likely explained by the use of different field sites, which can influence the nature of the low-frequency motion and amplitude of the large eddies that cause the instantaneous plume to meander across a receptor, thereby producing the intermittency effect.

The fluctuation intensity, i, is defined as $i^2 \equiv \overline{c'^2}/C^2$; $c' \equiv \chi - C$ is the concentration fluctuation, and $\overline{c'^2}$ is the mean-square fluctuation (or concentration variance). Overbars and primes denote time averages (over the sampling period) and departures therefrom, respectively. Crosswind profiles of the fluctuation intensity i are displayed in Fig. 5a for various nondimensional downwind distances, x/h, from the source. These measured profiles are qualitatively similar to those measured by other investigators (e.g., Hanna 1984; Sawford et al. 1985; Dinar et al. 1988; Mylne and Mason 1991). In particular, the lateral cross sections of i at $x/h = 24$ appear consistent with the results of Mylne and Mason (1991) and YKCBB measured at similar ranges (in both cases, plume centerline values of i of between 2 and 3 are observed at about 50- to 60-m range), although the present measurements

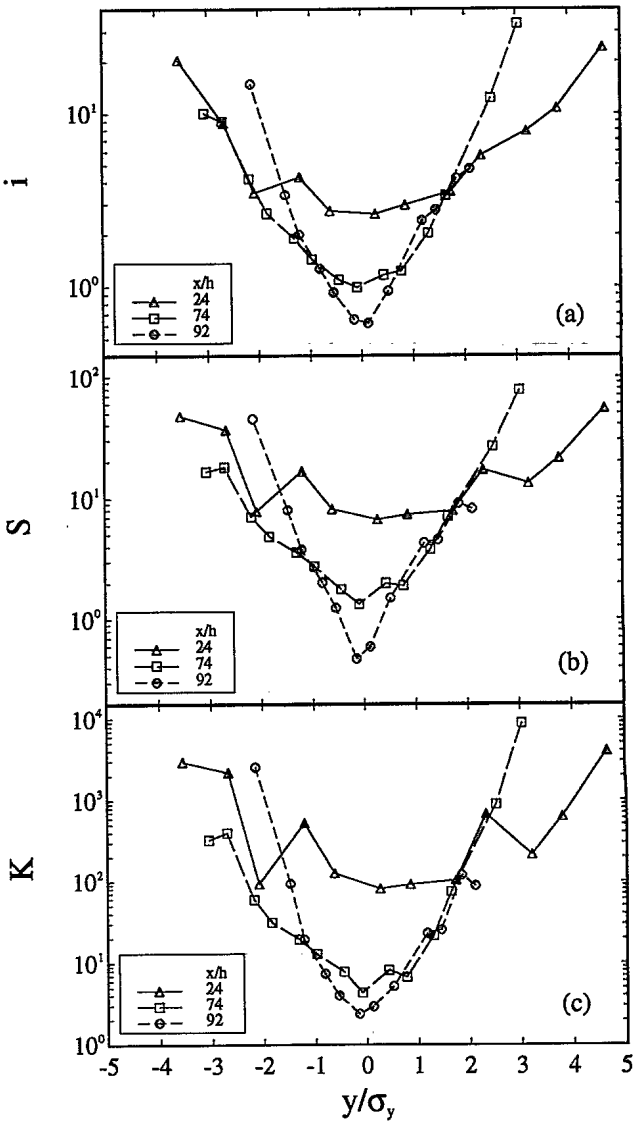

FIG. 5. Crosswind profiles of total (a) fluctuation intensity i, (b) skewness S, and (c) kurtosis K measured at three nondimensional downwind distances x/h.

extend the crosswind profiles out to larger normalized crosswind distances, y/σ_y. Interestingly, Mylne and Mason (1991) report a centerline value of i of about unity at 740 m, whereas our present experiments show an observed centerline i value of about 0.6 at a shorter range of 230 m (in spite of the much shorter averaging period of our detectors compared to those used by Mylne and Mason). The crosswind profiles of i exhibit an approximate bilateral symmetry about the mean plume centerline (i.e., about $y/\sigma_y = 0$). This implies that the mean wind directions were approximately perpendicular to the sampling line of concentration detectors for the examples shown in Fig. 5a.

Crosswind profiles of skewness $S \equiv \overline{c'^3}/(\overline{c'^2})^{3/2}$ and kurtosis $K \equiv \overline{c'^4}/(\overline{c'^2})^2$ are displayed in Figs. 5b

and 5c, respectively. The shapes of these profiles are qualitatively similar to those for the fluctuation intensity. The skewness profiles indicate that the concentration data are strongly skewed to the right. In general, the kurtosis is much larger than that from a Gaussian-distributed data sequence (where $K = 3$), indicating that the concentration data come from very peaked distributions. In summary, the lateral profiles of S and K show qualitatively similar patterns, with large positive deviations from Gaussian behavior (e.g., $S = 0$ and $K = 3$) observed throughout most of the plume. In broad terms, these features of S and K crosswind profiles are in qualitative agreement with those presented by YKCBB.

Conditional sampling of the concentration data to remove all intervals of zero concentration provides time series from which conditional (i.e., in-plume) concentration statistics can be obtained. Accordingly, crosswind profiles of conditional fluctuation intensity i_p, conditional skewness S_p, and conditional kurtosis K_p are shown in Figs. 6a, 6b, and 6c, respectively. As observed by other researchers (e.g., Sawford 1987; Dinar et al. 1988; Mylne and Mason 1991; YKCBB), the conditional statistics exhibit much less variation across a lateral plume cross section and are generally smaller in absolute value than the corresponding total statistics. Nevertheless, it can be seen that the conditional statistics appear to increase with increasing $|y|/\sigma_y$, and that this trend is more clear-cut for the profiles measured at the longer ranges (e.g., at $x/h = 74$ and 92), where the contribution of meandering to the fluctuations was becoming less important relative to the internal fluctuations of the plume.

Conditional fluctuation statistics reflect the nature of concentration fluctuations within the instantaneous (meandering) plume. The observed dependence of the conditional statistics on crosswind position suggests that the instantaneous plume is not similar at points within the plume cross section. The dependence of i_p on crosswind position in the current experiments at short range (e.g., $x/h = 24$) is stronger than those reported by Mylne and Mason (1991) and YKCBB at similar distances. Also, the present results show a much more substantial variation of i_p with crosswind position at longer ranges (e.g., $x/h = 74$ and 92) than those obtained by Mylne and Mason (1991) at similar or greater downwind distances (e.g., cf. Fig. 9 in Mylne and Mason with Fig. 6a). The differences may be caused by the extent of plume meandering present in the various field experiments. Indeed, in previous investigations by Mylne and Mason (1991) and YKCBB, i_p appeared to be approximately constant across a horizontal plume cross section, implying that most of the crosswind variation in the corresponding i can be attributed to variation in γ. The approximate constancy of i_p across a plume is a consequence of strong horizontal meandering, whereby points in the instantaneous plume are exposed uniformly to all sampling positions through the mean plume horizontal cross

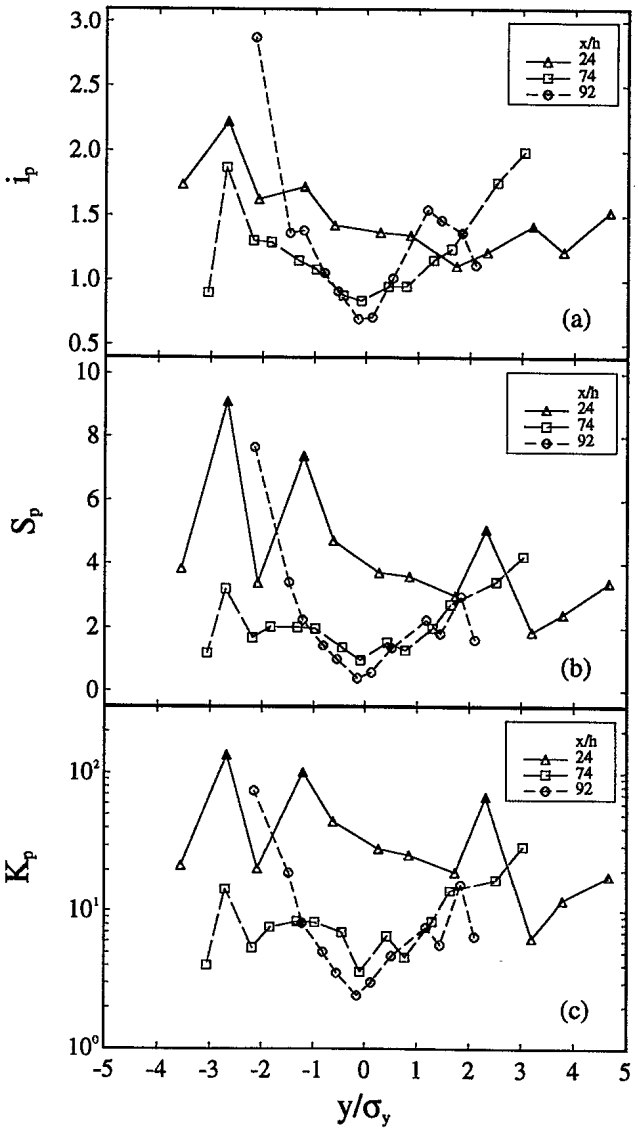

FIG. 6. Crosswind profiles of conditional (a) fluctuation intensity i_p, (b) skewness S_p, and (c) kurtosis K_p measured at three nondimensional downwind distances x/h.

section. In contrast, results obtained by Bara et al. (1992) in a water channel show a clear increase of i_p toward the edges of the plume from a minimum at the mean plume centerline. In the latter experiments, the horizontal meandering is reduced because of the much larger source size used and the restriction of the large-scale turbulent motions by the sidewalls of the water channel.

In spite of these differences, plume centerline values of 1.4, 3.3, and 24 for i_p, S_p, and K_p, respectively, measured at the 50-m range in YKCBB compare well with similar values measured at the 60-m range in the present study. Finally, plume centerline values of i_p, S_p, and K_p appear to decrease initially [e.g., cf. centerline values of i_p, S_p, and K_p measured at $x/h = 24$ with those measured at longer range ($x/h \geq 50$) in Fig. 6].

This initial decrease can probably be attributed to the increasing importance of continued molecular mixing, which smooths the internal plume structure leading to the progressive loss (dissipation) of finescale, high-frequency fluctuations in the plume at the longer ranges. Indeed, molecular diffusion (mixing) is the only physical process in the dispersing plume that can lead to a reduction in concentration gradients and peak concentrations in the plume (Chatwin and Sullivan 1979; Sawford and Hunt 1986).

c. *Concentration probability distribution*

The one-point concentration probability density function (PDF) provides the distribution of concentration values encountered at a fixed point in the dispersing plume and, in consequence, provides the statistical information required to predict the likelihood of concentrations exceeding critical thresholds above which they might be hazardous. The concentration PDF is important because it provides a more complete representation of the instantaneous concentration than the individual moments (e.g., mean, fluctuation intensity, skewness, kurtosis) considered earlier.

Histograms of the instantaneous concentration χ normalized by the mean concentration C were compiled by sorting the concentration data into bins and appropriately normalizing the bin counts to form the total PDF of concentration $f(\chi/C)$—that is,

$$\int_0^\infty f\left(\frac{\chi}{C}\right) d\left(\frac{\chi}{C}\right) = 1. \qquad (2)$$

PDFs of normalized concentration were determined to facilitate comparisons between the results for different positions in the plume. Figures 7 and 8 display the measured PDFs of χ/C at various crosswind positions in the plume for nondimensional downwind distances of $x/h = 24$ and 92, respectively. The PDF amplitudes in Fig. 7 are plotted on a logarithmic scale to better compare the large peaks at zero concentration and emphasize the upper tails. The very sharp and large peaks at zero concentration, however, are not plotted in Fig. 8 to emphasize the shape of the PDF at nonzero concentrations (and, in particular, to show the presence of the mode at nonzero concentration that is absent in the PDFs shown in Fig. 7). Figures 7 and 8 clearly show the variation in the shape of the concentration PDF as a function of both crosswind distance from the mean plume centerline and downwind distance from the source.

At $x/h = 24$, the PDFs of χ/C are strongly peaked at the origin and decay in an exponential-like tail away from it. Moving from the mean plume centerline to the fringes, the peak at zero concentration becomes more and more dominant (i.e., sharper and deeper), reflecting the changing shape of the PDF as the intermittency factor γ decreases from a value of approximately 0.26 near the plume centerline (i.e., at $|y|/\sigma_y \approx 0$) to a value less than 0.015 at the plume fringes (cf. Fig. 4b). The PDFs are skewed positively with heavy upper tails, and the most probable value (mode) is not the mean concentration because there is a high probability of detecting pollutant elements of small or zero concentration (viz., near a small source, plume meandering is a dominant mechanism for generating concentration fluctuations, and the amplitude variation of the zero concentration peak in the PDF through a plume crosswind cross section is directly attributable to the variation of γ). The upper tails of the concentration PDFs measured in the vicinity of the mean plume centerline (e.g., Figs. 7a and 7b) are flatter than exponential, while those of the PDFs measured toward the plume fringes (e.g., Figs. 7c and 7d) are well fit by an exponential over three to four decades of the probability scale.

Farther downwind at $x/h = 92$, the concentration PDFs near the mean plume centerline exhibit a bimodal form—a narrow sharp peak is observed at or near zero concentrations and a broad peak is observed at a higher nonzero concentration of $\chi/C \approx 1.5$ (cf. Figs. 8a and 8b). This mode at nonzero concentration is not present in the concentration PDFs observed at $x/h = 24$. Furthermore, we note that the peak near-zero concentration is genuine and cannot be attributed to noise in the measurements. Its amplitude and position are virtually unchanged before and after the noise removal used in the initial processing [cf. Eq. (1)]. Before any noise removal, the small contribution from the noise is indicated by the presence of very small PDF amplitudes (e.g., several orders of magnitude less than the peak at zero concentration) for concentrations less than 0 (recall that negative concentrations occur because the baseline level is adjusted to correspond to the mean level of the noise). Moving away from the mean plume centerline (e.g., as $|y|/\sigma_y$ increases), the probability of observing small concentrations increases because there is an increasing probability of encountering clean ambient air parcels. This is reflected in a concomitant decrease in the ratio of the amplitudes of the peaks corresponding to nonzero and zero concentrations as $|y|/\sigma_y$ increases. Hence, the bimodal form of the concentration PDF becomes weaker and weaker as $|y|/\sigma_y$ increases from 0 to approximately 1, after which the mode at nonzero concentration is no longer discernible (cf. Fig. 8c). Indeed, at the plume fringes (e.g., for $|y|/\sigma_y \gtrsim 2$), the PDF assumes an exponential-like shape with no mode whatsoever at a nonzero concentration (cf. Fig. 8d).

In this study, a unimodal form of the concentration PDF with a strong peak at zero concentration has been observed at short range (e.g., around 50 m). At ranges of between approximately 200 and 325 m, a bimodal form for the concentration PDF emerges at or near the mean plume centerline, possessing a dominant, sharp peak at zero concentration and a weak, broad peak at a nonzero concentration. Interestingly enough, the

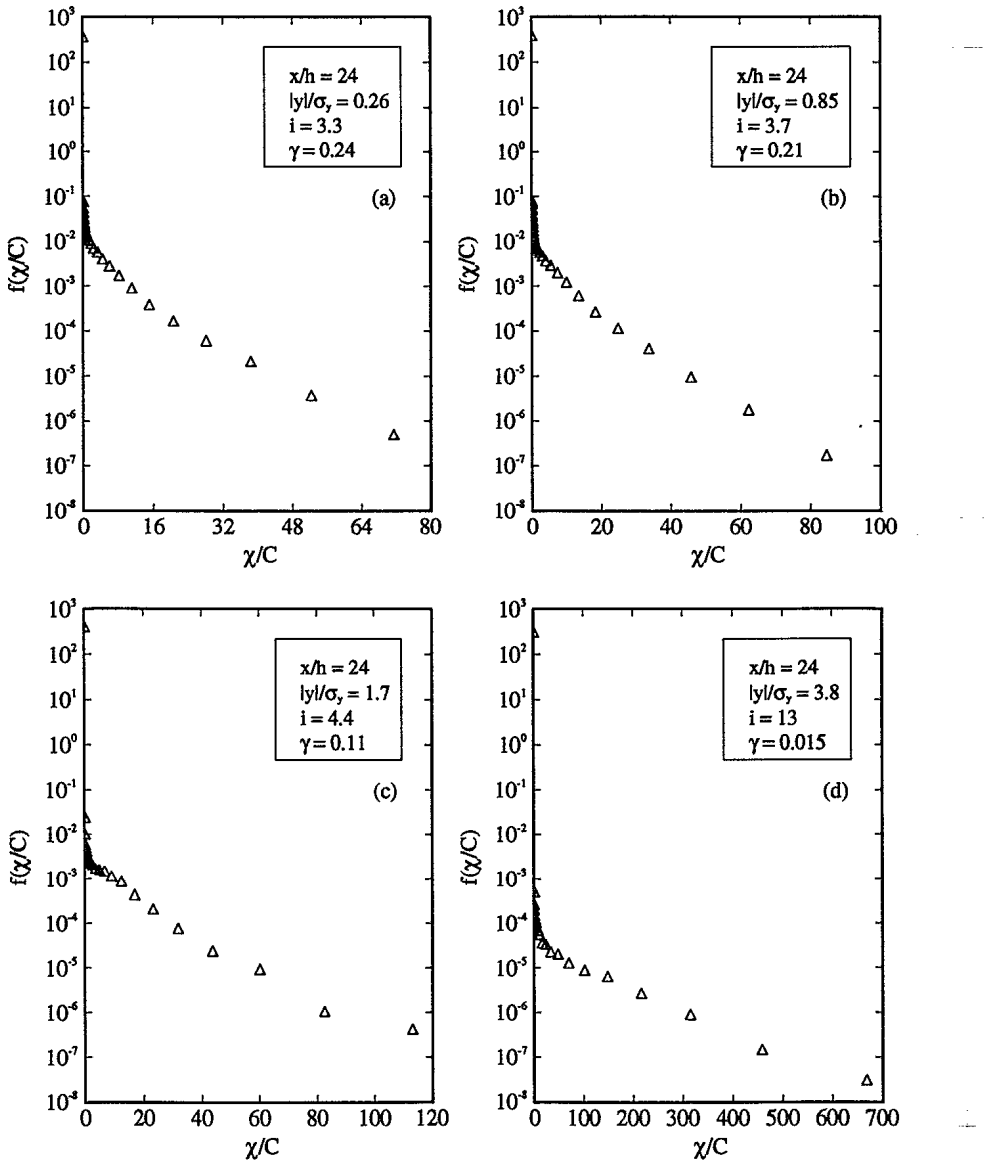

FIG. 7. Probability density function $f(\chi/C)$ of normalized concentration χ/C measured at various points in a crosswind cross section of a dispersing plume at the nondimensional downwind distance $x/h = 24$.

measurements of Mylne and Mason (1991) near the mean plume centerline at still longer ranges (e.g., around 750 m) seem to indicate that the bimodal form for the concentration PDF eventually transitions to a unimodal concentration PDF again but now with the peak at a nonzero concentration (cf. Mylne and Mason's Fig. 15, where the peak occurs at around $\chi \approx C$); the peak at zero concentration appears to have disappeared altogether as the asymptotic state of plume development is approached where the intermittency tends to one and the contaminant parcels in the plume are becoming well mixed.

It is known that the form of the concentration PDF is less sensitive to receptor location after removal of the intervals of zero concentration from the time series (e.g., after conditional sampling) (Sawford 1987). Figure 9 shows the measured conditional exceedance probability distributions of χ/C_p (the probability of exceeding concentration χ/C_p, where C_p is the conditional mean) for various positions in a crosswind cross section through the plume at $x/h = 24$ and 92. The profile of conditional distributions at $x/h = 24$ exhibits a change in shape through a horizontal plume cross section, but this change is considerably less than that observed for the corresponding profile of total concentration PDFs (cf. Figs. 7 and 9a). As in the case for the profiles for i_p, S_p, and K_p (cf. Fig. 6), the profile of conditional PDFs at $x/h = 24$ appears to show a

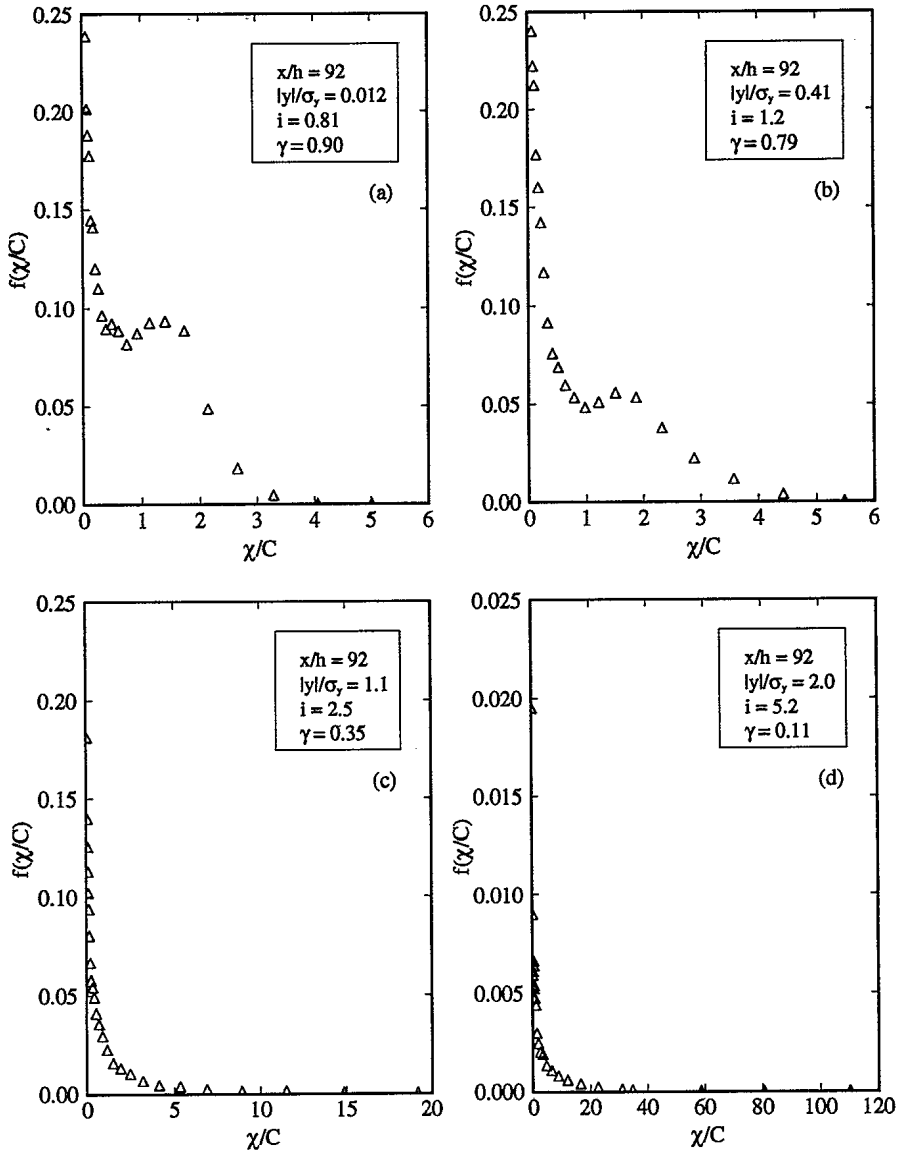

FIG. 8. Probability density function $f(\chi/C)$ of normalized concentration χ/C measured at various points in a crosswind cross section of a dispersing plume at the nondimensional downwind distance $x/h = 92$. Here, the large peak at zero concentration has not been plotted to emphasize the shape of the PDF at nonzero concentrations.

greater variation through a horizontal plume cross section than that measured by YKCBB at $x/h = 20$. Nevertheless, the conditional concentrations that are exceeded 1% of the time at the mean plume centerline at $x/h = 20$ as measured by YKCBB (cf. Fig. 9 in YKCBB) and at $x/h = 24$ as measured in the present study (cf. Fig. 9a) are about the same—namely, about $6.8C_p$. We note, however, that the profile of conditional PDFs at $x/h = 92$ exhibits a much greater change in shape across the lateral plume cross section than that at $x/h = 24$ (cf. Figs. 9a and 9b). Here, the probability distributions exhibit longer upper tails with increasing $|y|/\sigma_y$, an observation that is consistent with the general tendency for i_p, S_p, and K_p to increase with increasing $|y|/\sigma_y$ at $x/h = 92$ (cf. Fig. 6).

Figure 10 illustrates the change in shape with downwind distance of conditional concentration distributions measured near the mean plume centerline. Probability distributions measured at longer range exhibit shorter upper tails than those measured at shorter range (e.g., high in-plume concentrations are observed with smaller frequency at longer range). For example, the conditional concentration that is exceeded about 0.1% of the time at $x/h = 24$, 74, and 92 is approximately $11.6C_p$, $5.6C_p$, and $3.9C_p$, respectively. The shorter tails exhibited by the conditional PDFs at longer range can

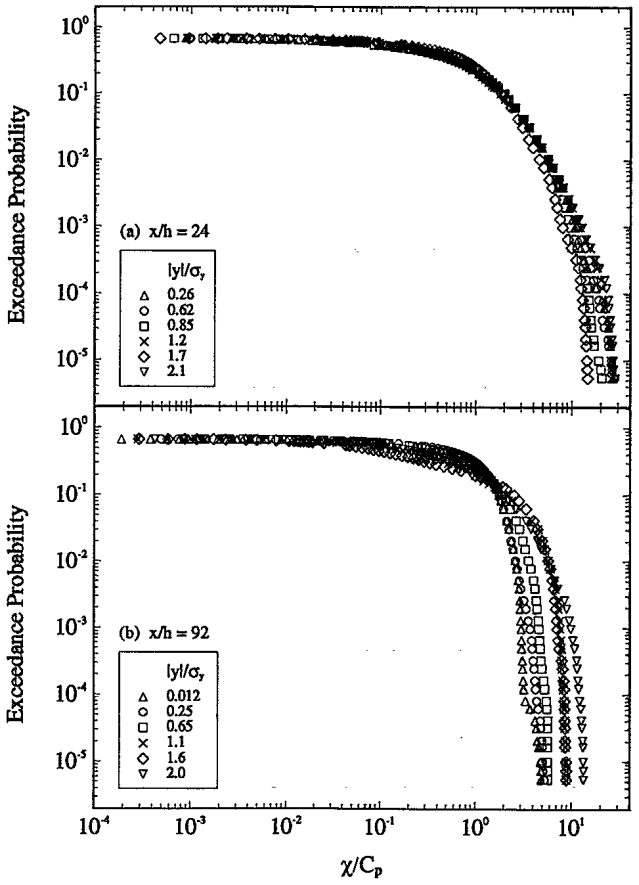

FIG. 9. Exceedance probability distributions of conditionally sampled and normalized concentration χ/C_p measured at various points in a crosswind cross section of a dispersing plume at nondimensional downwind distances (a) $x/h = 24$ and (b) $x/h = 92$.

probably be attributed to the continued molecular mixing that smooths the finescale and high-frequency structure in the plume. In other words, the plume appears to be more throughly mixed at longer range, and this feature is evident on comparison of the concentration time series in Figs. 2a and 3a.

YKCBB described methods for fitting a number of standard model PDFs [e.g., lognormal distribution (Csanady 1973); exponential distribution (Hanna 1984); clipped normal distribution (Lewellen and Sykes 1986); gamma distribution (Deardorff and Willis 1988)] to the observed conditional distributions as well as techniques to assess the quality of fit to the data based on quantile–quantile (QQ) plots. These methods have been applied to the concentration data obtained from Phase I of CONFLUX in YKCBB and to Phase II in the present paper. In YKCBB, it was found that none of the standard PDFs fit the data well over the entire range of positions in the plume (e.g., with a range of between 25 and 100 m in Phase I), and this conclusion has not been altered after an analysis of concentration data obtained from the longer-range field experiments undertaken during Phase II (e.g., with a range of between 50 and 325 m). Based on YKCBB and the present results, we found that generally the conditional concentration PDF, $f(\chi/C_p)$, was best modeled with the gamma distribution, particularly for downwind distances and atmospheric stability conditions in which the plume structure approached a more homogeneous state. This state was achieved either under stable stratification, when the plume structure appeared to be less fragmented and more coherent, or at a greater downwind range, when the contaminant parcels in the plume were more well mixed (i.e., from the continued action of molecular diffusion).

Finally, Yee et al. (1993c) showed that the change in shape of the total concentration PDF as a function of downwind distance, x/h, and crosswind position, y/σ_y, can be modeled using a meandering plume model with internal fluctuations. Here, it was demonstrated that a meandering plume model that explicitly incorporated the effects of small-scale structure in the instantaneous plume was able to reproduce many of the features observed in the total concentration PDF documented here. Furthermore, this physically based model led to a far greater diversity in shapes for the concentration PDF in a dispersing plume than is embodied in the simple PDF forms taken from elementary statistics (e.g., exponential, lognormal, clipped normal).

5. Temporal concentration statistics

a. Power spectra and autocorrelations

In this section, some results are presented from correlation and spectral analyses of the concentration fluctuation time series. The autocorrelation function $R(\tau)$ of the concentration time series at a fixed sampling point has its usual meaning here—that is,

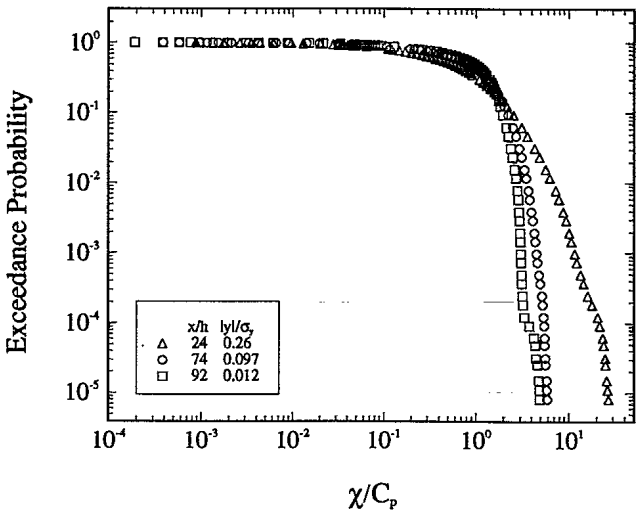

FIG. 10. Exceedance probability distributions of conditionally sampled and normalized concentration χ/C_p measured near the mean plume centerline at three nondimensional downwind distances x/h.

$$R(\tau) = \frac{\overline{[\chi(t) - C][\chi(t+\tau) - C]}}{\overline{[\chi(t) - C]^2}}, \qquad (3)$$

where $\chi(t)$ is the concentration time signal measured at time t, and τ is the correlation lag time.

Figure 11 exhibits sample autocorrelation functions $R(\tau)$ corresponding to the concentration time series shown in Figs. 2 and 3. The autocorrelation functions show the range of timescales that are responsible for the concentration patterns exhibited in Figs. 2 and 3. In Fig. 11a (measured in the vicinity of the mean plume centerline at $x/h = 24$), the autocorrelation function exhibits a small-lag-time portion that decays rapidly toward zero. This implies that the time interval over which the small-scale structures within the instantaneous plume remain well correlated is short (i.e., the plume timescale is short). This autocorrelation function is similar to those measured by Dinar et al. (1988), Mylne (1992), and YKCBB under near-neutral stability for downwind distances less than about 100 m. This form of the autocorrelation function is typical of the case where the entire instantaneous plume sweeps over the receptor a large number of times within the sampling period as the result of a nearly periodic meander component.

Figure 11c corresponds to an autocorrelation function that was measured near the mean plume centerline at $x/h = 92$. In this case, the initial decay toward zero is not as rapid as in Fig. 11a, implying that the high-frequency in-plume fluctuations remain correlated for a longer time (viz., the plume timescale is longer at the greater downwind location). At longer lag times, however, this autocorrelation function exhibits broad quasi-periodic secondary peaks that are associated with low-frequency plume meander. In this case, however, the scale of the horizontal plume meander was comparable to that of the instantaneous plume width, causing the instantaneous plume to meander back and forth over the receptor position without ever wandering off it (i.e., the plume was almost always present at the sampling point, as can be seen by examining Fig. 3a). Finally, Fig. 11d shows an autocorrelation function measured off the mean plume centerline at $x/h = 92$. Here, at longer lag times, the autocorrelation exhibits a number of sharp and quite prominent secondary peaks that are much more pronounced than those found in an autocorrelation measured near the mean plume centerline at the same downwind distance. In this case, the autocorrelation pattern is typical of the case where only the fringes of the instantaneous plume are impacting a receptor located near the outer limits of the plume meander, generating a series of concentration bursts (cf. Fig. 3b) whose decorrelation and recorrelation as a function of lag time produce the multiple peaks in the autocorrelation function of Fig. 11d. It is interesting to note that the myriad of forms in the autocorrelation function that we have observed in the dispersing plume are similar qualitatively (if not quantitatively) with the correlation features predicted using a sinusoidal meandering plume model (Peterson et al. 1990).

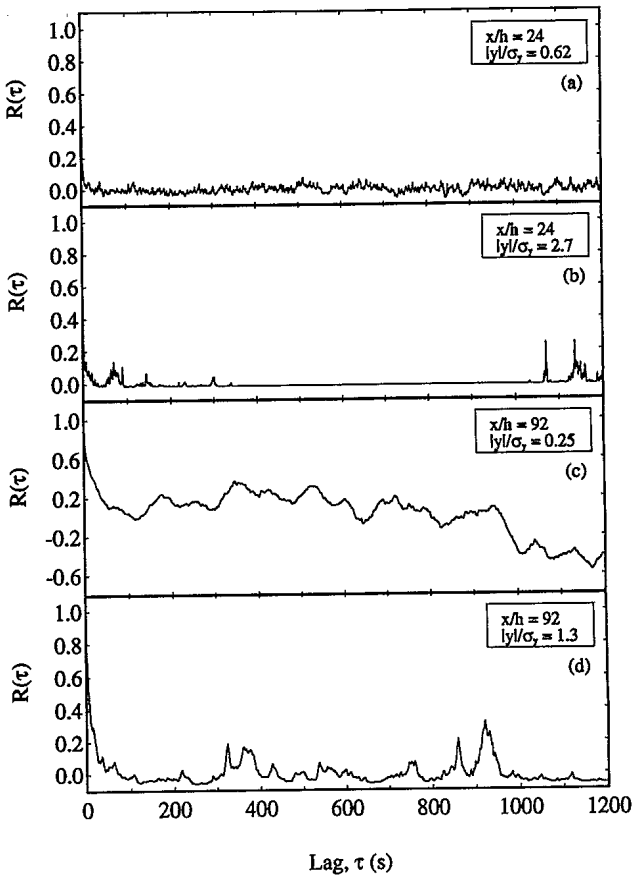

FIG. 11. Sample autocorrelation function of concentration time series measured at (a) $x/h = 24$, $|y|/\sigma_y = 0.62$; (b) $x/h = 24$, $|y|/\sigma_y = 2.7$; (c) $x/h = 92$, $|y|/\sigma_y = 0.25$; and (d) $x/h = 92$, $|y|/\sigma_y = 1.3$.

Figure 12 exhibits power spectral densities of concentration fluctuations measured near the mean plume centerline (where the intermittency factor was as large as possible) at several downwind distances under a variety of atmospheric stability conditions. The sample concentration spectra have been extracted from various experiments conducted during both Phase I and II of CONFLUX. Figure 12 depicts $S(n)$ scaled by n/σ_χ^2 on the vertical axis and n scaled by the local value of σ_y/U on the horizontal axis. Here, $S(n)$ is the concentration power spectrum, $\sigma_\chi^2 \equiv \overline{c'^2}$ is the concentration variance, and n is the frequency (Hz). The overall normalization for $S(n)$ was selected so that

$$\int_0^\infty S(n)dn = \sigma_\chi^2.$$

The scaling for the concentration power spectrum used in Fig. 12 was suggested by Hanna and Insley (1989). There is a moderate collapse of power spectra obtained using this scaling, but the power spectra certainly do

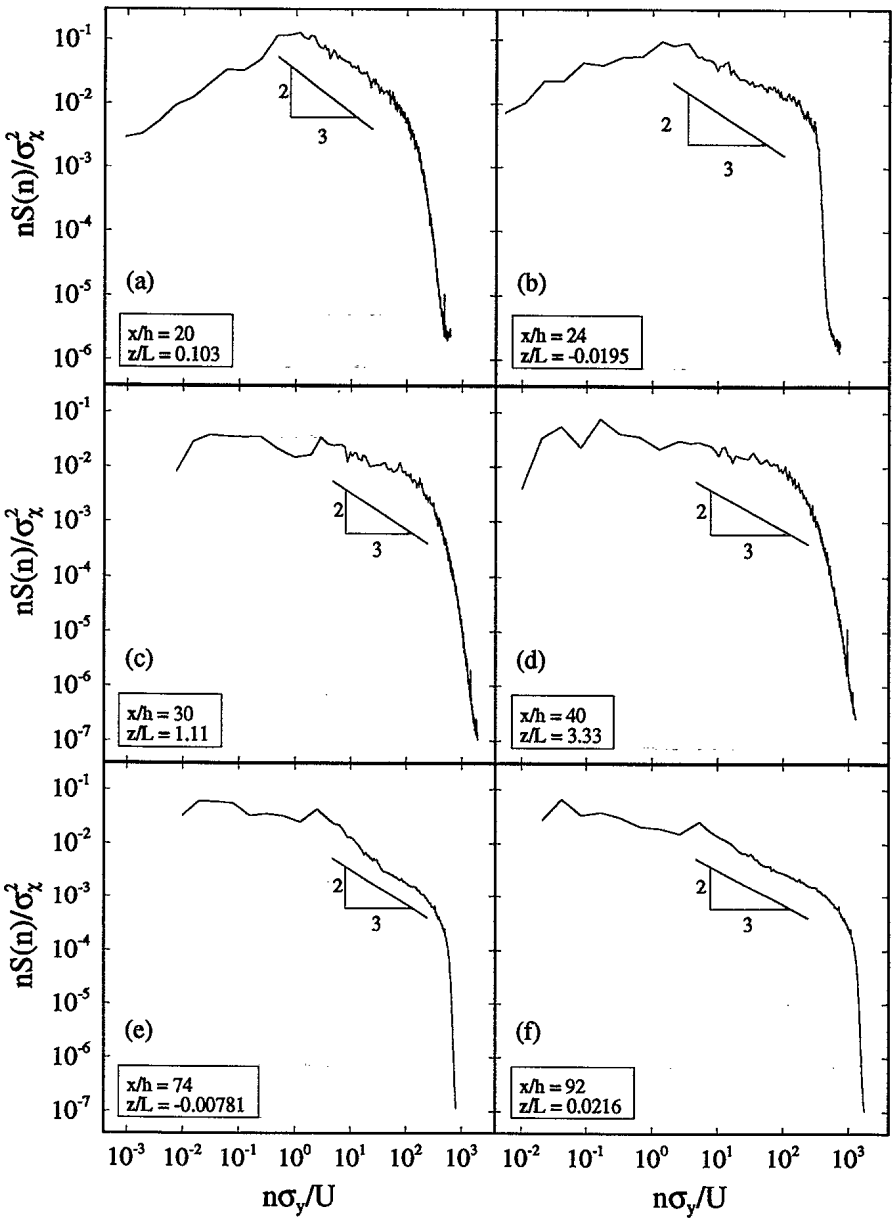

FIG. 12. Sample concentration power spectra measured at various downwind distances and atmospheric stability conditions. The straight line, corresponding to a slope of $-2/3$, shows the extent of the inertial-convective subrange.

not collapse upon a universal curve. Furthermore, there appears to be no apparent functional relationship between the ordering of the spectra based on amplitude and atmospheric stability as embodied in the stability parameter z/L.

The concentration power spectra are composed of three subranges: the variance-production subrange, the inertial-convective subrange, and the dissipation subrange. The dissipation subrange in which the spectra are affected by the process of molecular diffusion is beyond the temporal resolution of our concentration detectors, and this inadequate instrument performance is reflected in the steep spectral roll-off in the power spectra for $n\sigma_y/U \geq 200$. In Fig. 12, a line having a slope of $-2/3$ has been included to indicate the extent of the inertial-convective subrange. Most of the concentration power spectra are seen to exhibit a significant $-5/3$ power-law region [i.e., $nS(n) \sim n^{-2/3}$] spanning about two decades from $n\sigma_y/U \approx 3$ to 100. This region corresponds to the inertial-convective subrange associated with the range of scales at which concentration variance is transferred from large to small scales with no production or dissipation. As noted by Mylne and Mason (1991), this range is associated with those frequencies that correspond to scales of motion that are small relative to the instantaneous plume width. In

consequence, Mylne and Mason (1991) remarked that their detectors were not sufficiently responsive to resolve the inertial-convective subrange for concentration spectra measured at ranges less than 100 m under near-neutral conditions, although this subrange was clearly evident in their spectra measured at longer ranges (e.g., at several hundred meters), where the plume timescales were longer. Using our faster-response detectors, the inertial-convective subrange is clearly evident even in concentration spectra measured at the shorter ranges (cf. Figs. 12a and 12b) under approximately neutral stability.

Interestingly, we note that concentration spectra measured under extreme stable stratification (e.g., cf. Fig. 12d, where $z/L = 3.33$) do not appear to exhibit a well-defined region where the spectral slope obeys the $-5/3$ power law, in contrast to spectra measured under either near-neutral or slightly stable stratification at the same downwind range (e.g., cf. Fig. 12d with Fig. 20 in YKCBB). This may indicate that under extreme stable stratification, there is a short circuit of the concentration variance cascade that transfers fluctuation variance from large to small scales, implying that internal mixing processes within the plume may have been suppressed. Indeed, under very strong stable stratification, the buoyant suppression of turbulent stirring and active mixing in the plume may ultimately alter the fluctuation variance cascade.

The low-frequency end of the concentration spectra corresponds to the variance-production region (e.g., $n\sigma_y/U \lesssim 1$) and shows greater variability in behavior than the inertial-convective subrange. Indeed, the low-frequency end of $S(n)$ embodies information on the large-scale eddies and the effects of meandering of the horizontal wind direction, and, in consequence, these eddies would not be expected to have a structure of universal form in contrast to the inertial-convective eddies. Because the inherent statistical scatter in the spectral amplitude estimates is larger at the lower frequencies (viz., a low-frequency component contributes fewer cycles of motion over which to average in any given fixed sampling period) and hence can lead to ambiguities in interpretation, it is necessary to be cautious in the interpretation of features in the low-frequency end of the concentration spectrum. With this caveat in mind, we note that some of the concentration spectra appear hump shaped and exhibit a single broad peak at $n\sigma_y/U \approx 1$, marking the beginning of the inertial-convective subrange (e.g., cf. spectra shown in Figs. 12a and 12b).

If frequency is not normalized by mean plume width, σ_y, the spectral peak frequency marking the beginning of the inertial-convective subrange was generally found to shift toward lower frequencies with increasing downwind distance from the source. This observation is consistent with results reported by Mylne and Mason (1991) and YKCBB.

b. *Upcrossing interval and excursion duration probability distributions*

The instantaneous concentration time series $\chi(t)$ exhibits an upcrossing of the mean concentration level C at time t_0 if $\chi(t_0)$ crosses the constant level C with positive slope. Similarly, $\chi(t)$ exhibits a C downcrossing at time t_0 if $\chi(t_0)$ crosses the mean concentration level with negative slope. The duration of an excursion about the mean concentration level is defined as the time interval between an upcrossing and the subsequent downcrossing of C. The time interval t_u between successive upcrossings of the mean concentration and the excursion duration t_e about the mean concentration were extracted from the concentration time series by locating and marking data points whenever they crossed the mean concentration level and identifying the slope as positive or negative. Probability density functions $f(t_u)$ and $f(t_e)$ were then generated from the upcrossing time intervals and excursion durations. The upcrossing interval and excursion duration statistics characterize the concentration time signal as a series of discrete events (i.e., an episodic perspective), rather than as a superposition of harmonic waves as in spectral analysis (i.e., a harmonic perspective).

Figure 13 shows the crosswind variation of the PDF of upcrossing intervals, $f(t_u)$, over the mean concentration level for two downwind positions, $x/h = 24$ and 92. The PDFs measured across the plume at each downwind location collapse down quite well. Departures from a perfect collapse occur in the extreme upper tails, where there is a higher probability of observing longer upcrossing intervals at the plume fringes because the plume is more intermittent there. For example, at $x/h = 92$, upcrossing intervals greater than approximately 100 s are not observed near the mean plume centerline, but upcrossing intervals as large as 600 s are observed at the plume edges ($|y|/\sigma_y \approx 2$). The sharp turn in the tails of the PDF for $t_u \gtrsim 100$ s is easily understood. Because the upcrossing intervals are bounded above by the sampling time, the upper tails of the upcrossing interval PDFs must terminate at finite values.

If the concentration time signal was periodic, $f(t_u)$ would reduce to a single Dirac delta function located at the period of the wave. Any randomness in shape and arrival of the concentration pulses would result in a broadening of any peak in $f(t_u)$. The upcrossing interval PDFs exhibit a single broad probability peak—the most probable upcrossing interval (mode) is found to be ≈ 0.006 s. For $t_u \gtrsim 0.006$ s, $f(t_u)$ exhibits a power law $f(t_u) \sim t_u^{-p}$, where the exponent p has an almost constant value of $8/5$ for all positions in the dispersing plume. This power law fits the upcrossing interval PDF over five to six decades of the probability scale. The upcrossing intervals determine the times between successive concentration bursts. The observation that the time between two concentration bursts follows a power-

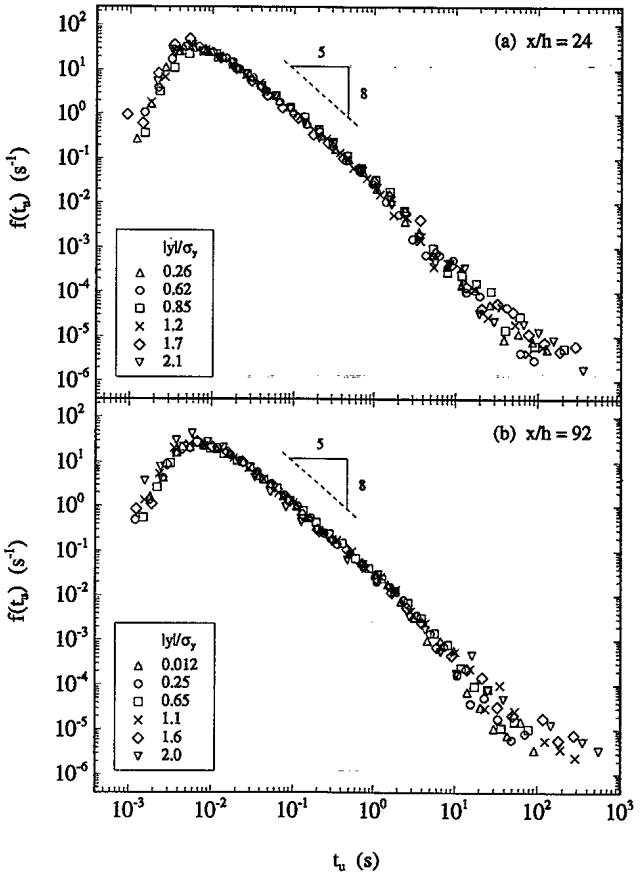

FIG. 13. Probability density function $f(t_u)$ of upcrossing intervals t_u over the mean concentration measured at various points in a crosswind cross section of the plume at nondimensional downwind distances (a) $x/h = 24$ and (b) $x/h = 92$. The dashed line, corresponding to a slope of $-8/5$, indicates the extent of the power-law region for $f(t_u)$.

law distribution rather than an exponential distribution implies that these bursts do not occur randomly in time and are not independent of each other.

Figure 14 shows the PDF of excursion durations $f(t_e)$ measured at various points in a crosswind direction through the plume at two downwind locations. The collapse of the excursion duration PDFs upon a single curve is limited to the shorter excursion times corresponding to the smaller-scale structures in the plume. Nevertheless, the collapse of $f(t_e)$ in this region is very good, suggesting that the form of the corresponding small-scale plume structures remains the same as a function of crosswind and downwind position in the plume. The most probable excursion duration occurs at about 0.003 s. For excursion durations approximately greater than or equal to 0.003 s, $f(t_e)$ follows a power-law distribution [i.e., $f(t_e) \sim t_e^{-r}$ with an exponent r of about $3/2$ that is independent of the observation point in the plume]. Again, it is noted that the power-law part of the PDF is extensive, spanning a range of over five decades on the PDF scale. The distribution of excursion durations reflects the range of persistence times of concentration bursts that pass by the receptor position. In this regard, we note that near the mean plume centerline, an excursion duration as long as approximately 10 s is observed at $x/h = 92$, in contrast with a maximum excursion duration of 3 s measured at $x/h = 24$. This suggests that the characteristic timescales of the in-plume fluctuations are longer at greater downwind distances. This behavior is consistent with an increase in the plume timescale with increasing downwind fetch, as observed in the time required for the initial decline of the sample autocorrelation function (e.g., cf. Figs. 11a and 11c). All these observations are consistent with a visual examination of the time series displayed in Figs. 2a and 3a, in which it is quite evident that concentration bursts at $x/h = 24$ appear to be short, whereas those at $x/h = 92$ appear to be more prolonged (i.e., consist of longer periods of sustained nonzero concentrations).

In YKCBB, the distribution of gap and burst durations in concentration fluctuation data was determined (viz., respectively, upcrossing intervals and excursion durations referenced to the zero concentration

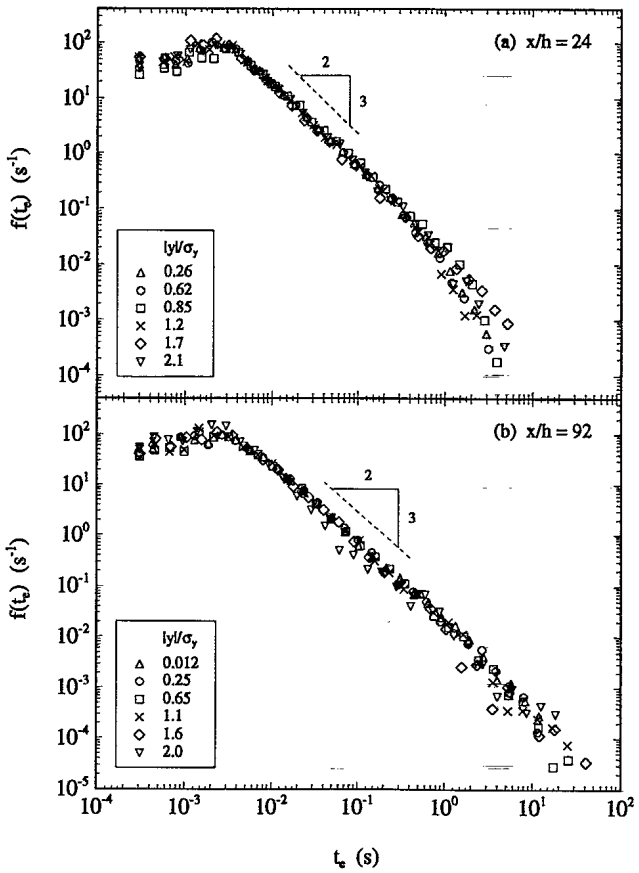

FIG. 14. Probability density function $f(t_e)$ of excursion durations t_e over the mean concentration measured at various points in a crosswind cross section of the plume at nondimensional downwind distances (a) $x/h = 24$ and (b) $x/h = 92$. The dashed line, corresponding to a slope of $-3/2$, indicates the extent of the power-law region for $f(t_e)$.

level, rather than the mean concentration level considered in the present study). Here, it was found that the burst duration distribution also followed a power-law distribution, but with a power-law exponent of $-7/5$, which is different from the exponent of $-3/2$ determined for the excursion duration (about the mean concentration) PDF (cf. Fig. 14 with Figs. 16 and 17 in YKCBB). The dynamical characteristics in a dispersing plume that are responsible for the change in the distribution shape of upcrossing intervals and excursion durations about various fixed concentration levels are not known at this time. It is conceivable that simple modeling concepts such as the meandering plume model developed by Peterson et al. (1990) may lead to further understanding of this phenomenon. A more extensive study of these level-crossing distributions is certainly warranted in view of their importance in practical applications (e.g., Kristensen et al. 1989; Yee et al. 1993b).

c. *Timescales, length scales, and microscales*

A number of timescales can be extracted from the concentration time series. Toward this objective, we define the following timescales:

(i) A correlation timescale T_χ of concentration fluctuations can be determined from the autocorrelation function $R(\tau)$ as follows:

$$T_\chi = \int_0^{\tau_*} R(\tau)d\tau, \tag{4}$$

where τ_* is the e-folding time for the autocorrelation function [viz., the time lag when $R(\tau)$ first falls below e^{-1}, so τ_* is the lag time such that $R(\tau_*) = e^{-1}$]. For our data, the usual integral timescale found by integrating the autocorrelation function over the entire range of lag times [e.g., $\tau \in [0, \infty)$] does not exist because the autocorrelation function generally does not decay to zero at long lag times. Indeed, in certain cases, the large-scale meandering motion (i.e., large compared to the scale of the instantaneous plume width) introduces a low-frequency component in the measured concentration time series that produced quasioscillations in the autocorrelation function that are sustained even at long lag times (cf. Fig. 11).

(ii) A timescale T_P can be derived from the inverse of the frequency at the spectral peak:

$$T_P = n_m^{-1}, \tag{5}$$

where n_m is the frequency corresponding to the peak of the concentration power spectrum.

(iii) Two physically meaningful timescales can be derived from the statistics of upcrossing intervals and excursion durations about the mean concentration, where

$$T_u = \overline{t_u} \tag{6}$$

is the expected or mean time interval between successive upcrossings of the mean concentration, and

$$T_e = \overline{t_e} \tag{7}$$

is the expected or mean excursion duration from the mean concentration.

(iv) The Taylor microtimescale T_T is defined as

$$T_T \equiv \left[\frac{2\overline{c'^2}}{(\partial\chi/\partial t)^2}\right]^{1/2} = \left[\frac{-2}{d^2R(\tau)/d\tau^2}\right]^{1/2}_{\tau\to 0}. \tag{8}$$

The microtimescale is evaluated by fairing a smooth cubic-spline approximation to the observed autocorrelation function near zero lag using generalized cross-validation to estimate the smoothing parameter (Craven and Wahba 1979) and then evaluating the second derivative of the computed spline at zero lag (calculating the limit curvature of the autocorrelation function as $\tau \to 0$). We stress that the Taylor microscale measured here is appropriate for concentration time signals measured by our detectors and as such is conditioned by the time constant implicit in the instrumental averaging. In consequence, the values of the Taylor microscale considered here are not for the unfiltered concentration signal (viz., the signal for which the finest scales in the dispersing plume have been resolved). Indeed, the Taylor microscale for the unfiltered concentration time series is undoubtedly considerably smaller because of the extreme reduction and sensitivity of the concentration derivative variance [cf. (8)] to instrumental smoothing (Yee et al. 1993b).

It is more appropriate to consider physical length scales of motion related to turbulent concentration eddy sizes in the plume rather than timescales, because timescales at a fixed receptor position in a plume are dependent on the mean wind speed U and as such become shorter as U increases. Using Taylor's "frozen flow" approximation, the timescales defined previously can be converted to various length scales of the plume by normalization with the mean wind speed U: $\Lambda_\chi = UT_\chi$ is the correlation length scale; $\Lambda_P = UT_P$ is the length scale based on the spectral peak; $\Lambda_u = UT_u$ is the length scale associated with the mean spacing between concentration bursts; $\Lambda_e = UT_e$ is the length scale associated with the mean size of concentration bursts; and $\Lambda_T = UT_T$ is the Taylor micro–length scale. We note that the Taylor micro–length scale, Λ_T, does not represent the average size of the dissipative eddies, which is of the order of the Batchelor length scale $\lambda_B \equiv (D^2\nu/\epsilon)^{1/4}$ [ν is the kinematic viscosity of air, D is the molecular diffusivity of the scalar (propylene) in air, and ϵ is the mean viscous dissipation rate]. For the case of diffusion of propylene into air, the Schmidt number $\mathrm{Sc} \equiv \nu/D \approx 1$, so the Batchelor length scale at which molecular diffusion in the concentration field becomes important is comparable to the Kolmogorov length scale, $\lambda_K \equiv (\nu^3/\epsilon)^{1/4}$, at which viscous dissipation in the velocity field becomes important.

At a fixed downwind distance, Λ_e, Λ_T, and Λ_χ were found to be approximately constant across a crosswind plume cross section. These three length scales are microscales that are determined primarily by the small-scale molecular mixing and turbulent stirring in the plume (i.e., by the internal mixing processes within the plume). In contrast, the length scales Λ_P and Λ_u exhibit variations in a lateral cross section through the plume. As an example, Fig. 15 shows the crosswind variation of Λ_u at several downwind locations. As would be expected, Λ_u, which reflects the mean spacing between concentration pulses, increases toward the plume fringes, where the intermittency is lower. Length scales Λ_P and Λ_u are affected by the large-scale meandering motions of the plume, and this is mirrored by the variation in the crosswind distribution of these scales. In consequence, the latter scales contain information on plume meandering but embody little information on the small-scale mixing processes in the plume. Interestingly, we found that the behavior of the correlation scale Λ_χ is generally different than that of the length scale derived from the spectral peak, Λ_P. This difference may be attributed to Λ_χ being an integral estimate of the separation distance at which concentration fluctuation measurements within the plume remain well correlated, whereas Λ_P reflects the dominant length scale associated with the concentration fluctuations (which in many cases would be determined by the longer meander timescale).

The downwind development of the various length scales along the mean plume centerline is presented in Fig. 16. Here, the length scales have been normalized by the mean plume crosswind dispersion σ_y. The data have been taken from a number of field experiments conducted during both Phase I and II of CONFLUX and encompass a variety of downwind distances, intermittency factors, and atmospheric conditions. With the exception of Λ_χ, all length scales are found to increase roughly proportionally with σ_y. Interestingly, normalization of length scales by the mean plume dispersion allows comparisons between results for different stratification strengths (viz., the normalized length scale is only weakly dependent on the stability parameter z/L). Although there is considerable scatter in the data points (the spread ranges from an octave to a decade for the measured length scales), the Taylor and excursion duration length scales appear to be smaller than the spectral-peak length scale, with the upcrossing interval length scale (Λ_u) intermediate between these two sets of scales. The smallest length scale of the group is the Taylor microscale.

Interestingly, the correlation length scale Λ_χ increases with downwind fetch x at a rate that is somewhat faster than the growth of σ_y (cf. Fig. 16a). In particular, a least-squares fit of Λ_χ with x shows that $\Lambda_\chi/\sigma_y \sim (x/h)^{3/2}$. It is unclear what physical processes in the dispersing plume are associated with the length scale Λ_χ. The timescale T_χ may be associated with the characteristic time taken for the dominant-sized concentra-

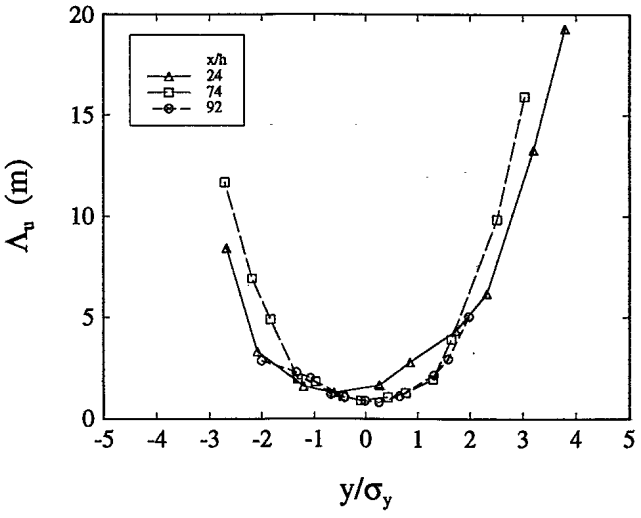

FIG. 15. Crosswind profiles of the upcrossing interval length scale Λ_u measured at three nondimensional downwind distances x/h.

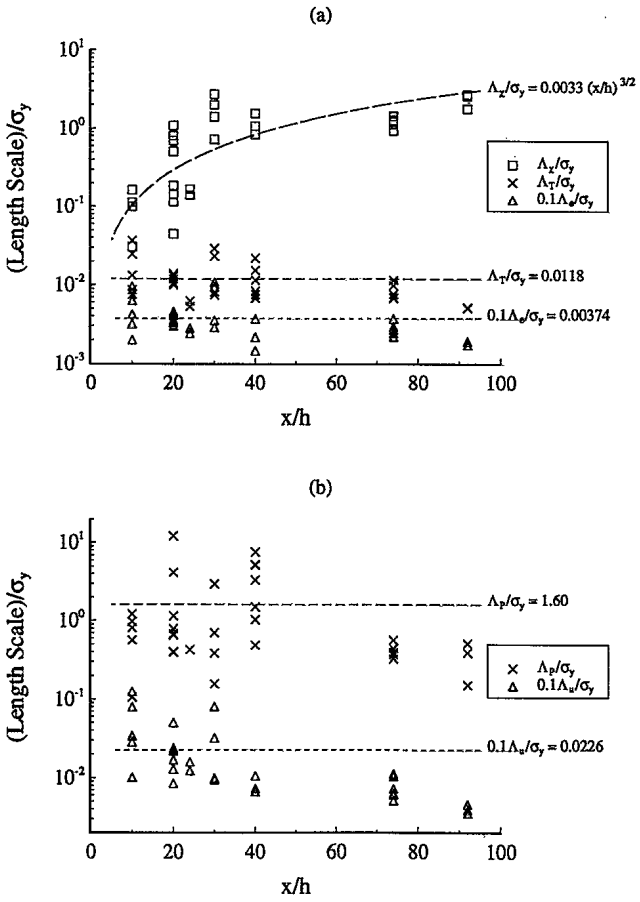

FIG. 16. Downwind development of a number of length scales that have been normalized by the mean plume dispersion σ_y. The length scales are the correlation scale Λ_χ, the Taylor microscale Λ_T, the excursion duration scale Λ_e, the spectral peak scale Λ_P, and the upcrossing interval scale Λ_u.

tion eddies within the instantaneous plume to be advected by the mean wind past the receptor position in the alongwind direction (and hence, as mentioned earlier, may represent the timescale over which concentrations fluctuations in the plume remain well correlated). If so, $T_\chi \sim \sigma_i/U$, and $\Lambda_\chi/\sigma_y \sim \sigma_i/\sigma_y$, where σ_i denotes the instantaneous plume width. Close to the source, the standard deviation of lateral concentration distribution in the plume grows linearly (i.e., $\sigma_y \sim x$). If we adopt the relative diffusion law of Richardson (1926) so $\sigma_i \sim x^{3/2}$, this implies that $\Lambda_\chi/\sigma_y \sim (x/h)^{1/2}$. This is at variance, however, with our observation that Λ_χ/σ_y grows at a much greater rate [e.g., $\sim(x/h)^{3/2}$].

Finally, we consider the velocity-to-concentration field scale ratio

$$\Pi \equiv \frac{2k/\epsilon}{U^2T_T^2/12D}, \qquad (9)$$

where Π is the ratio of the timescale of the turbulent velocity field, $2k/\epsilon$ (which is the ratio of turbulent kinetic energy of velocity fluctuations to the mean viscous dissipation rate), to a timescale of the concentration field, $U^2T_T^2/12D$ (which is based on the Taylor microscale). The molecular diffusivity D of propylene in air was estimated from the correlation relationships given in Reid et al. (1987). Here, $k \equiv 0.5(\sigma_u^2 + \sigma_v^2 + \sigma_w^2)$ is the turbulent kinetic energy of velocity fluctuations and was obtained directly from the sonic anemometer data. The turbulent kinetic energy (TKE) dissipation rate ϵ was determined from

$$\epsilon = \frac{u_*^3}{\kappa z}\Phi_\epsilon\left(\frac{z}{L}\right), \qquad (10a)$$

where u_* is the friction velocity, κ is von Kármán's constant ($\approx$0.4), and $\Phi_\epsilon(z/L)$, the dimensionless profile of TKE dissipation rate in the diabatic surface layer, is given by

$$\Phi_\epsilon\left(\frac{z}{L}\right) = 1 - \frac{z}{L}, \quad \frac{z}{L} \leqslant 0 \qquad (10b)$$

for unstable and neutral conditions (Panofsky and Dutton 1984) and

$$\Phi_\epsilon\left(\frac{z}{L}\right) = \left[1 + 2.5\left(\frac{z}{L}\right)^{0.6}\right]^{3/2}, \quad \frac{z}{L} > 0 \qquad (10c)$$

for stable conditions (Wyngaard and Coté 1971).

Figure 17 shows the downwind development of Π near the mean plume centerline. The velocity-to-concentration timescale ratio appears to attain a nearly constant asymptotic value of approximately 0.35 for $x/h \gtrsim 30$ (at least over the downwind range covered by our measurements). The concentration data used to construct Fig. 17 were extracted from field experiments conducted during Phase I and II of CONFLUX, and as such they encompass a broad range of atmospheric stratification ($-0.15 \leqslant z/L \leqslant 3.0$). Given the statistical scatter in the determination of Π, we judged that there was no major difference in the velocity-to-concentration timescale ratio that can be attributed to atmospheric stability (at least over the range of atmospheric stratification covered by our data).

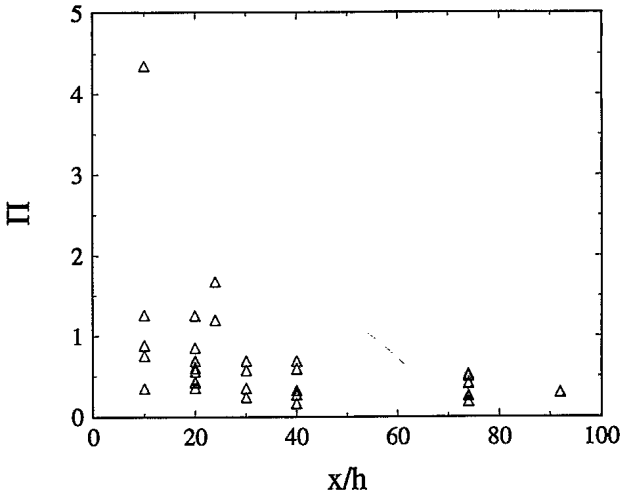

FIG. 17. Downwind development of the velocity-to-concentration timescale ratio Π.

6. Conclusions

The amplitude and temporal statistics of concentration fluctuations in a plume dispersing from a point source in the atmospheric surface layer have been measured with a very fast response concentration detector. The main conclusions of the present study can be summarized as follows:

1) Crosswind profiles of i, S, and K are approximately symmetric in a crosswind plume cross section about the mean plume centerline. This symmetry reflects the approximately stationary mean wind speed and direction and turbulence characteristics of the atmosphere over the sampling period. Mean plume centerline values of γ are nondecreasing with downwind distance, at least over the range of x/h between approximately 10 and 130 represented by our data. Crosswind profiles of i_p, S_p, and K_p are found to exhibit a dependence on crosswind position (e.g., they exhibit a minimum at the plume centerline and increase toward the fringes), but this crosswind variation is much less pronounced than that observed in the corresponding total statistics. The crosswind variation of i_p, S_p, and K_p in a horizontal plume cross section is more significant at longer ranges, where meandering is less important.

2) The shape of the total concentration PDF depends strongly on crosswind and downwind location in the plume. Close to the source in the meander-dominated regime of plume development, the concentration

PDF appears exponential-like with a large peak at zero concentration associated with plume intermittency due to meandering; this mode at zero concentration increases as the receptor position moves off the mean plume centerline, reflecting the greater probability of finding unmixed ambient (i.e., clean) air at the plume fringes. Farther downwind in the regime of plume development where contributions of plume meandering and internal structure to fluctuations are comparable, the total concentration PDF on the plume axis becomes bimodal; the peak at zero concentration reflects the intermittency due to plume meandering, and the secondary peak at nonzero concentrations reflects the contribution of the in-plume structure. At even greater downwind distances, in the turbulent-diffusive regime of plume development where contributions of internal fluctuations are becoming dominant, the concentration PDF on the plume centerline assumes a unimodal form again, but now with a peak at a nonzero concentration [results of Mylne and Mason (1991) seem to indicate that this mode occurs at $\chi \approx C$].

3) The concentration power spectra measured at various positions in the plume and under a variety of atmospheric stability conditions exhibit a moderate collapse when a scaling proposed by Hanna and Insley (1989) is applied, but this collapse is far from perfect. The spectra measured under near-neutral to slightly stable stratification exhibit an extensive inertial-convective subrange (i.e., an approximate $-5/3$ power-law region) spanning approximately two decades in frequency. The frequency marking the beginning of the inertial-convective subrange decreases (i.e., the extent of the inertial-convective subrange increases) with increasing downwind fetch. The downwind variation of this frequency is consistent with the usual picture of successive cascades to the Batchelor scale in the plume, which must necessarily scale with the instantaneous plume width σ_i at which the cascade begins. Concentration spectra measured under extreme stable stratification (where turbulence energy levels are very low as a result of suppression of turbulent motions by the buoyancy forces) do not appear to support a clear inertial-convective subrange, implying a short circuit of the fluctuation variance cascade under these conditions.

4) The PDFs of upcrossing intervals and excursion durations over the mean concentration, measured at a number of crosswind and downwind positions in the plume under a variety of atmospheric stability conditions, are approximately self-similar when attention is confined to the shorter upcrossing intervals and excursion times (e.g., timescales associated with the small-scale structures in the dispersing plume). The most probable values of upcrossing intervals and excursion durations over the local mean concentration level were 0.006 and 0.003 s, respectively, independent of position in the dispersing plume. Beyond these modes, the PDFs of upcrossing intervals and excursion durations are well approximated by power laws with power exponents $-8/5$ and $-3/2$, respectively, over about five to six decades of the probability scale. These PDFs embody information on the temporal structure of the finescale in-plume motions. Approximate self-similarity of these PDFs at the smaller scales implies that the small-scale structures at all points in a dispersing plume are approximately geometrically similar.

5) With the exception of the correlation scale, concentration length scales grow in proportion to the mean plume width σ_y with downwind fetch. This implies that the influence of time and space averaging on concentration fluctuations would be reduced with increasing downwind fetch.

REFERENCES

Bara, B. M., D. J. Wilson, and B. W. Zelt, 1992: Concentration fluctuation profiles from a water channel simulation of a ground-level release. *Atmos. Environ.*, **26A,** 1053–1062.

Biltoft, C. A., 1991: Concentration fluctuation modeling of chemical hazards. Field test at U.S. Army Dugway Proving Ground, Dugway, Utah, 96 pp. [Available from Defence Scientific Information Service, Department of National Defence, Ottawa, Ontario, Canada K1A 0K2.]

Chandler, G. M., 1991: Development of fast-response tracer gas sensors for use in full-scale atmospheric dispersion field trials. Part I: Hardware component. Part II: Field testing component. Tech. Rep. for Defence Research Establishment Suffield, S & J Engineering, Inc., Scarborough, Ontario, 82 pp. [Available from Scientific Information Section, Defence Research Establishment Suffield, P.O. Box 4000, Medicine Hat, AB Canada T1A 8K6.]

——, 1993: Development of fast-response tracer gas sensors for use in full-scale atmospheric dispersion field trials. Hardware improvements. Tech. Rep. for Defence Research Establishment Suffield, S & J Engineering, Inc., Scarborough, Ontario, 116 pp. [Available from Scientific Information Section, Defence Research Establishment Suffield, P.O. Box 4000, Medicine Hat, AB Canada T1A 8K6.]

Chatwin, P. C., 1982: The use of statistics in describing and predicting the effects of dispersing gas clouds. *J. Hazard Mater.*, **6,** 213–230.

——, and P. J. Sullivan, 1979: The relative diffusion of a cloud of passive contaminant in incompressible turbulent flow. *J. Fluid Mech.*, **91,** 337–355.

——, and ——, 1989: The intermittency factor of scalars in turbulence. *Phys. Fluids A,* **1,** 761–763.

——, and ——, 1993: The structure and magnitude of concentration fluctuations. *Bound.-Layer Meteor.*, **62,** 269–280.

Craven, P., and G. Wahba, 1979: Smoothing noisy data with spline functions. *Numerische Mathematik,* **31,** 377–403.

Csanady, G. T., 1967: Concentration fluctuations in turbulent diffusion. *J. Atmos. Sci.*, **24,** 21–28.

——, 1973: *Turbulent Diffusion in the Environment.* D. Reidel Publishing Company, 248 pp.

Deardorff, J. W., and G. E. Willis, 1988: Concentration fluctuations within a laboratory convectively mixed layer. *Lectures on Air Pollution Modeling,* A. Venkatram and J. C. Wyngaard, Eds., Amer. Meteor. Soc., 357–384.

Dinar, N., H. Kaplan, and M. Kleiman, 1988: Characterization of concentration fluctuations of a surface plume in a neutral boundary layer. *Bound.-Layer Meteor.*, **45,** 157–175.

Fackrell, J. E., and A. G. Robins, 1982a: Concentration fluctuations and fluxes in plumes from point sources in a turbulent boundary layer. *J. Fluid Mech.*, **117,** 1–26.

——, and ——, 1982b: The effects of source size on concentration fluctuations in plumes. *Bound.-Layer Meteor.*, **22,** 335–350.

Gifford, F. A., 1959: Statistical properties of a fluctuating plume dispersion model. *Advances in Geophysics,* Vol. 6, Academic Press, 117–137.

Hanna, S. R., 1984: The exponential probability density function and concentration fluctuations in smoke plumes. *Bound.-Layer Meteor.,* **29,** 361–375.

——, and E. M. Insley, 1989: Time series analysis of concentration and wind fluctuations. *Bound.-Layer Meteor.,* **47,** 131–147.

Kristensen, L., J. C. Weil, and J. C. Wyngaard, 1989: Recurrence of high concentration values in a diffusing, fluctuating scalar field. *Bound.-Layer Meteor.,* **47,** 263–276.

Lewellen, W. S., and R. I. Sykes, 1986: Analysis of concentration fluctuations from lidar observations of atmospheric plumes. *J. Climate Appl. Meteor.,* **25,** 1145–1154.

Mole, N., 1990: A model of instrument smoothing and thresholding in measurements of turbulent dispersion. *Atmos. Environ.,* **24A,** 1313–1323.

Mylne, K. R., 1992: Concentration fluctuation measurements in a plume dispersing in a stable surface layer. *Bound.-Layer Meteor.,* **60,** 15–48.

——, and P. J. Mason, 1991: Concentration fluctuation measurements in a dispersing plume at a range of up to 1000 m. *Quart. J. Roy. Meteor. Soc.,* **117,** 177–206.

Panofsky, H. A., and J. A. Dutton, 1984: *Atmospheric Turbulence.* John Wiley, 397 pp.

Pasquill, F., and F. B. Smith, 1983: *Atmospheric Diffusion.* 3d ed. John Wiley, 429 pp.

Peterson, H., B. Lamb, and D. Stock, 1990: Interpretation of measured tracer concentration fluctuations using a sinusoid meandering plume model. *J. Appl. Meteor.,* **29,** 1284–1299.

Reid, R. C., J. M. Prausnitz, and B. E. Poling, 1987: *The Properties of Gases and Liquids.* 4th ed. McGraw-Hill Book Company, 741 pp.

Richardson, L. F., 1926: Atmospheric diffusion shown on a distance-neighbor graph. *Proc. Roy. Soc. London A,* **110,** 709–737.

Sawford, B. L., 1987: Conditional concentration statistics for surface plumes in the atmospheric boundary layer. *Bound.-Layer Meteor.,* **38,** 209–223.

——, and J. C. R. Hunt, 1986: Effects of turbulence structure, molecular diffusion and source size on scalar fluctuations in homogeneous turbulence. *J. Fluid Mech.,* **165,** 373–400.

——, C. C. Frost, and T. C. Allan, 1985: Atmospheric boundary-layer measurements of concentration statistics from isolated and multiple sources. *Bound.-Layer Meteor.,* **31,** 249–268.

Stapountzis, H., B. L. Sawford, J. C. R. Hunt, and R. E. Britter, 1986: Structure of the temperature field downwind of a line source in grid turbulence. *J. Fluid Mech.,* **165,** 401–424.

Wyngaard, J. C., and O. R. Coté, 1971: The budgets of turbulent kinetic energy and temperature variance in the atmospheric surface layer. *J. Atmos. Sci.,* **28,** 190–201.

Yee, E., P. R. Kosteniuk, G. M. Chandler, C. A. Biltoft, and J. F. Bowers, 1993a: Statistical characteristics of concentration fluctuations in dispersing plumes in the atmospheric surface layer. *Bound.-Layer Meteor.,* **65,** 69–109.

——, ——, ——, ——, and ——, 1993b: Recurrence statistics of concentration fluctuations in plumes within a near-neutral atmospheric surface layer. *Bound.-Layer Meteor.,* **66,** 127–153.

——, R. Chan, P. R. Kosteniuk, G. M. Chandler, C. A. Biltoft, and J. F. Bowers, 1994: Incorporation of internal fluctuations in a meandering plume model of concentration fluctuations. *Bound.-Layer Meteor.,* **67,** 11–39.

148750

NO. OF COPIES NOMBRE DE COPIES	COPY NO. COPIE Nº	INFORMATION SCIENTIST'S INITIALS INITIALES DE L'AGENT D'INFORMATION SCIENTIFIQUE
1	1	
AQUISITION ROUTE ▶ FOURNI PAR	DRES	
DATE ▶	12 Dec 94	
DSIS ACCESSION NO. ▶ NUMÉRO DSIS		

DND 1158 (6-87)

National Defence / Défense nationale

PLEASE RETURN THIS DOCUMENT TO THE FOLLOWING ADDRESS:

DIRECTOR
SCIENTIFIC INFORMATION SERVICES
NATIONAL DEFENCE
HEADQUARTERS
OTTAWA, ONT. - CANADA K1A 0K2

PRIÈRE DE RETOURNER CE DOCUMENT À L'ADRESSE SUIVANTE:

DIRECTEUR
SERVICES D'INFORMATION SCIENTIFIQUES
QUARTIER GÉNÉRAL
DE LA DÉFENSE NATIONALE
OTTAWA, ONT. - CANADA K1A 0K2